



A Multi-Frequency Focused Impedance Measurement System Based on Analogue Synchronous Peak Detection

Muhammad Abdul Kadir¹, Adrian J. Wilson^{2,3} and K. Siddique-e Rabbani^{1*}

¹Department of Biomedical Physics and Technology, University of Dhaka, Dhaka, Bangladesh, ²Department of Physics, University of Warwick, Coventry, United Kingdom, ³Department of Clinical Physics and Bioengineering, University Hospital, Coventry, United Kingdom

OPEN ACCESS

Edited by:

Pedro Bertemes-Filho,
Santa Catarina State University, Brazil

Reviewed by:

Hassan Yazdani,
K.N.Toosi University of
Technology, Iran
Panagiotis Kassanos,
Imperial College London,
United Kingdom

*Correspondence:

K. Siddique-e Rabbani
rabbani@du.ac.bd

Specialty section:

This article was submitted to
Bioelectronics,
a section of the journal
Frontiers in Electronics

Received: 07 October 2021

Accepted: 23 November 2021

Published: 10 December 2021

Citation:

Kadir MA, Wilson AJ and
Siddique-e Rabbani K (2021) A Multi-
Frequency Focused Impedance
Measurement System Based on
Analogue Synchronous
Peak Detection.
Front. Electron. 2:791016.
doi: 10.3389/felec.2021.791016

Monitoring of anatomical structures and physiological processes by electrical impedance has attracted scientists as it is noninvasive, nonionizing and the instrumentation is relatively simple. Focused Impedance Method (FIM) is attractive in this context, as it has enhanced sensitivity at the central region directly beneath the electrode configuration minimizing contribution from neighboring regions. FIM essentially adds or averages two concentric and orthogonal combinations of conventional Tetrapolar Impedance Measurements (TPIM) and has three versions with 4, 6, and 8 electrodes. This paper describes the design and testing of a multi-frequency FIM (MFFIM) system capable of measuring all three versions of FIM at 8 frequencies in the range 10 kHz–1 MHz. A microcontroller based multi-frequency signal generator and a balanced Howland current source with high output impedance (476 k Ω at 10 kHz and 58.3 k Ω at 1 MHz) were implemented for driving currents into biological tissues with an error <1%. The measurements were carried out at each frequency sequentially. The peak values of the amplified voltage signals were measured using a novel analogue synchronous peak detection technique from which the transfer impedances were obtained. The developed system was tested using TPIM measurements on a passive RC Cole network placed between two RC networks, the latter representing skin-electrode contact impedances. Overall accuracy of the measurement was very good (error <4% at all frequencies except 1 MHz, with error 6%) and the resolution was 0.1 Ω . The designed MFFIM system had a sampling rate of >45 frames per second which was deemed adequate for noninvasive real-time impedance measurements on biological tissues.

Keywords: electrical bioimpedance, multi-frequency bioimpedance, FIM, bioinstrumentation, impedance spectroscopy, focused impedance method

INTRODUCTION

Bioimpedance is an emerging technique for monitoring anatomical structures and physiological processes. Recent studies demonstrated the use of bioimpedance techniques in different applications including cancer detection (Cheng et al., 2020; Mansouri et al., 2020; Tidy and Brown, 2021), tissue hydration (Lukaski et al., 2019), body composition (Vermeiren et al., 2021), vascular fluid flow (Anand et al., 2021) and bedside monitoring (Mulasi et al., 2015; Morais et al., 2021).

Conventional electrical impedance measurements use a bipolar configuration in which potential developed across two terminals in a network are measured for a specified driven current. This scheme is not suitable for bioimpedance measurements since tissue-electrode contact impedances are included in the measurement. Most bioimpedance measurement schemes use a Tetrapolar Impedance measurement (TPIM) technique where separate pairs of electrodes are used for current drive and potential measurement. The ratio of the measured voltage to the current is known as the transfer impedance and is a property of the bulk without any significant contribution from tissue-electrode contact impedances (Brown et al., 2000a; Martinsen and Grimnes, 2009). Typically, a voltage controlled current source having a very high output impedance is used so that tissue-electrode contact impedances in the current drive loop do not alter the current significantly. On the other hand, tissue-electrode contacts that are on the path of the potential measurement circuit loop do not drop any significant voltage since the input impedance of the voltage measurement circuit is very high, resulting in negligible current through this loop. Thus, TPIM essentially eliminates the tissue-electrode impedances and is also the basis of more sophisticated measurement techniques including the Focused Impedance Method (FIM), instrumentation for which is the subject of this paper, and electrical impedance tomography (EIT). The coinage of the term “transfer impedance” makes it distinct from “impedance” that is obtained in a bipolar measurement. However, use of ‘impedance’ in the bioimpedance literature essentially should be taken to mean “Transfer Impedance.” The above also implies that contact resistances of any switching circuitry at the electrodes will not affect the transfer impedance measurement.

The extent to which a change in resistivity of a point within a homogeneous volume conductor contributes to the change in measured transfer impedance is defined as the sensitivity (Geselowitz, 1971; Grimnes and Martinsen, 2008). The sensitivity distribution of the tetra-polar configuration extends to a large distance within the volume conductor and may not be suitable for identifying localized changes in impedivity (Brown et al., 2000a). Electrical Impedance Tomography (EIT, initially termed Applied Potential Tomography–APT) generates cross sectional images of the impedance distribution within the body using a number of electrodes, typically 8, 16, or 32, fixed circumferentially around the body and can localize changes in impedivity (Barber et al., 1984; Brown, 2003; Adler and Boyle, 2017) on the electrode plane. Reconstructing 2D EIT images is challenging although solutions have been developed (Holder, 2004) and EIT systems utilising these developments are now commercially available, primarily for respiratory imaging. However, since current flows in 3D, there is significant contribution to the image from points in the 3rd dimension (Rabbani and Kabir, 1991; Rabbani et al., 1996). Thus, the individual pixel values of the reconstructed image do not give an accurate value of the impedivity at that point in the medium. Several groups have undertaken efforts to obtain 3D EIT images having more of the above set of electrodes in several planes along

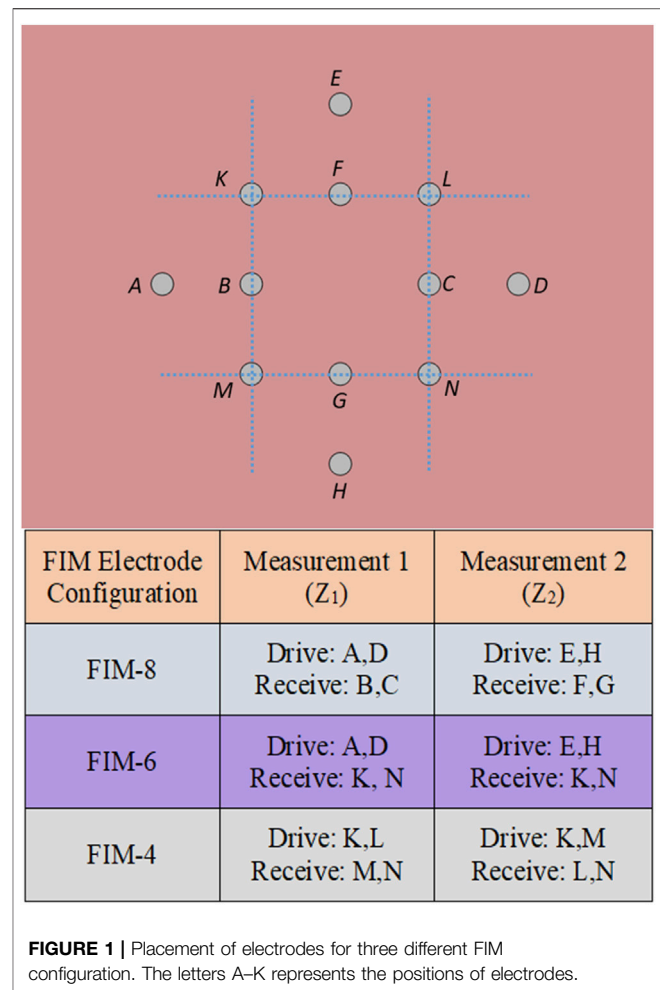


FIGURE 1 | Placement of electrodes for three different FIM configuration. The letters A–K represents the positions of electrodes.

the length of the cylinder (Ye et al., 2008; Hao et al., 2017; Zhang et al., 2019). However, reconstructing 3D EIT images is far more challenging than that for 2D images, and it will be quite some time before practically usable 3D EIT systems are developed for routine use. The limitations of EIT together with the complexity of the technology clearly identifies the need for a simpler method that can identify and localize impedivity changes. For localized impedance information in a volume conductor, a new measurement technique termed *Focused Impedance Method (FIM)* has been developed (Rabbani et al., 1999; Rabbani and Karal, 2008). FIM essentially consists of two concentric and orthogonal TPIM arrangements with the two transfer impedance measurements added or averaged. FIM has enhanced sensitivity in the central region of the electrode configuration with minimum contribution from neighboring regions in comparison to TPIM (Islam et al., 2010; Pettersen et al., 2014; Rabbani, 2018). Due to 3D sensitivity in a volume conductor, FIM may probe body organs at shallow depths using surface electrodes. There are three electrode configurations for FIM: 1) 8-electrode FIM (FIM-8), 2) 6-electrode FIM (FIM-6), and 3) 4-electrode FIM (FIM-4) (Rabbani et al., 1999; Rabbani and Karal, 2008). **Figure 1** represents the placement of electrodes on the surface of a volume conductor with the corresponding

drive receive electrode pairs for the three different FIM configurations. FIM has been useful in the study of gastric emptying (Rabbani et al., 1999), lung ventilation (Kadir et al., 2015) and abdominal fat thickness (Surovy et al., 2012). Finite element simulation and some phantom studies demonstrated the utility of FIM in the investigation of both epithelial (Kadir and Rabbani, 2018) and deep tissues (Roy et al., 2019). However, it should be noted that unlike impedance imaging, the electrode array needs to be manually repositioned to localize impedivity changes.

Childhood lung diseases like pneumonia and tuberculosis are common in developing countries (Izadnegahdar et al., 2013; Jenkins, 2016). Being a non-invasive and low cost technique, there is a potential of using multi-frequency FIM (MFFIM) in the study of these diseases. There is also a potential for using multi-frequency FIM for biological tissue characterization. However, a multi-frequency FIM system for bioimpedance measurements on human body has not been implemented and in this study, it is considered for the first time. Commercial devices are available for both TPIM and EIT but none for FIM measurements at present. Devices meant for TPIM (Bioscan-II; Sciospec) can be used for FIM measurements by manually changing the drive and receive electrode pairs, but this does not form a practical measurement technique; the whole measurement needs to be automated, giving the possibility of real-time measurement of dynamic processes. Considering the socio-economic status of low resource countries low cost, portable and reliable systems are required that can be maintained and repaired by local technicians. However, the limited availability of even quite basic electronic components in such environments is a challenge. The aim of this work was to develop a multi-frequency FIM system using widely available electronic components. This paper describes the design and development of a multi-frequency FIM system capable of measuring bioimpedance using all the three electrode configurations shown in **Figure 1** over a range of frequencies using microcontrollers and a PC, under software control, which also allows instant data recording and storage.

MATERIALS AND METHODS

FIM measurements are essentially based on Tetrapolar Impedance Measurements (TPIM), with the electrode configurations selected electronically. There are three major parts in an FIM device: current drive circuitry, voltage measurement circuitry and appropriate electrode switching as shown in **Figure 1**. A microcontroller based balanced current source was constructed for driving alternating current into biological tissues. The measured voltage gives the impedance and a change in impedance appears as a change of the voltage amplitude, which needs to be measured in real time. This was performed using *analogue synchronous peak detection* and its implementation for a multi-frequency device is explained. Design aspects of the switching circuitry together with necessary algorithms for measurement of all three versions of FIM (FIM-8, FIM-6, and FIM-4) are described. The performance of the implemented MFFIM device is measured using passive

component phantoms. Much of the basic instrumentation required for current injection and voltage measurement is standard and well described previously (e.g. Holder, 2004). We include our designs for these for completeness and to describe the impact restricted component selection criteria had on implementing an FIM measurement system.

Design Considerations

The frequencies and current used for impedance measurements must not cause changes to the tissue. For this reason, dc currents which can cause burns and electrolysis (Leeming et al., 1970; Dechent et al., 2020) are not used. Similarly, the current threshold for nerve stimulation is lowest for low frequency currents (0.1–500 Hz), rising rapidly as the frequency increases above 1 kHz. At frequencies above 1 MHz, stray capacitance becomes a significant problem, becoming very significant for instrumentation at GHz frequencies (Bolton et al., 1998; McEwan et al., 2007). Fortunately, the impedance of body tissues has significant dependence on the intermediate (kHz–MHz) range of frequencies that provide the opportunity to devise reasonably simple instrumentation. For example, the impedivity of inflated lung increases by 46 and 38% compared to that for a deflated lung for frequencies of 10 kHz and 1 MHz, respectively, (Gabriel et al., 1996). The variation of impedance over the frequency range 10 kHz–1 MHz is different for normal and diseased body tissues giving the possibility of tissue characterization using bioimpedance, which may be useful in diagnosis (Brown et al., 2000b). Therefore, the frequency range 10 kHz–1 MHz was chosen for the excitation signal of the implemented multi-frequency FIM system. To measure the impedance response over the entire frequency range 10 kHz–1 MHz, the system was designed for 8 octave related frequencies which are 10, 20, 40, 80, 160, 320, 640 and 1,024 kHz; a complete measurement “frame” would consist of measurements at all these frequencies. However, the highest measurement frequency implemented (1,024 kHz) was not an octave multiple of its previous frequency; it was a practical maximum that could be achieved using the available electronic components. The octave progression of measurement frequency gave equidistant points in the frequency range on a logarithmic scale.

In-vivo, FIM injects a current into the human body. In terms of maximizing the signal-to-noise ratio of the final system this needs to be as high as possible, but its effect on the body cannot be ignored. The International Electrotechnical Commission (IEC) defined the safe auxiliary current limit for medical equipment to be 100 μA (rms)/kHz (IEC, 2004). According to the *American National Standard*, safe auxiliary current limits for electromedical apparatus is 5 mA at 10 kHz; with higher currents (maximum limit 10 mA) being deemed safe at higher frequencies (AAMI, 1993). At higher frequencies, tissue heating (Joule heating) is the limiting factor. Tissue heating depends on a number of factors including: current density, time of exposure and blood flow in the tissue. For surface electrodes, current densities less than 1 mA/ mm^2 are unlikely to cause damage (Brown et al., 2017). Therefore, the maximum current of the MFFIM was specified to be 0.5 mA.

The measured voltage depends not only on electrical properties of the tissue sample under investigation, but also on

TABLE 1 | Design requirements for the multi-frequency FIM system.

Feature	Specification
Excitation frequency	10–1024 kHz
Drive current amplitude	0.5 mA
Current drive output impedance	>50 k Ω at 1 MHz >200 K Ω at 10 kHz
Transfer impedance range	5–100 Ω
Frame rate	>10 fps

the excitation current amplitude and the electrode configuration. Based on measurements from 12 normal human subjects, (Brown et al., 1994) reported that for a typical electrode configuration that they used, transfer impedance values of the human thorax were $(24.56 \pm 4.09) \Omega$ and $(15.70 \pm 2.80) \Omega$ at frequencies of 9.6 and 614.4 kHz, respectively. Again, the transfer impedance in the breast tissue, measured using four 7 mm diameter electrodes configured at the corners of a 4 cm square arrangement, varied between 5 and 50 Ω in the frequency range 5–200 kHz (Al Amin et al., 2014). Therefore, the transfer impedance range was specified as 5–100 Ω in the present work.

Electrical properties of some tissues/organs, including the lung and the heart change with time with different periodicities. In the case of the thorax, lung impedance changes slowly with breathing while cardio-vascular changes are faster. Therefore, a complete “frame” of multi-frequency measurements containing measurements at all 8 frequencies with FIM electrode switching, should be performed fast enough to allow dynamic measurement of the fastest change. Typically, the respiratory rate in a normal adult is 12–18 breaths-per-minute and the cardiac rate is 60–72 bpm, the latter increasing on exercise and with disease to a maximum of a little above 200 bpm. Therefore, the frame rate should be more than double this latter value if one wants to study cardiac related changes. That means the sampling frame rate should be greater than 400 fpm (frame per minute) or about 7 fps (frame per second). This frame rate will naturally cover changes with respiration which are much slower. Keeping some margin, the frame rate was specified to be greater than 10 fps in the present work.

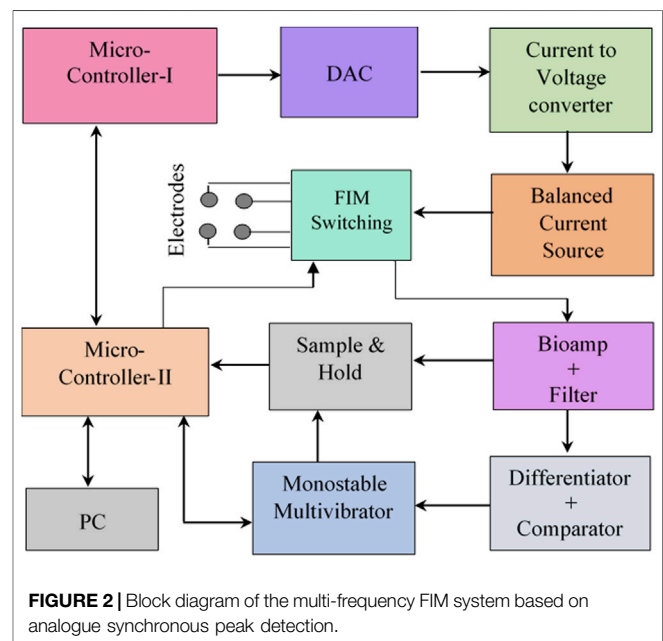
For the design for the constant amplitude current source, its output impedance has to be made very high compared to that of the driven load so that the current remains essentially constant irrespective of typical variations in the load impedance. Here the driven load impedance is that between two electrodes fixed to a human body which is essentially the sum of two electrode-tissue contact impedances and the bulk impedance of the body between these electrodes. Typical value of an electrode tissue contact impedance at 10 kHz is around 1–2 k Ω (McEwan et al., 2007) and that at 1 MHz is less than 500 Ω (Nguyen et al., 2013; Yang et al., 2017). The bulk impedance is expected to be of the order of the measured transfer impedance in a TPIM system, differing slightly depending on the position of the current and potential electrodes. The transfer impedance, considered for this design as mentioned before, was between 5 and 100 Ω , the lower values being typical for around 1 MHz while the higher value for around 10 kHz. Both of these are very small compared to the

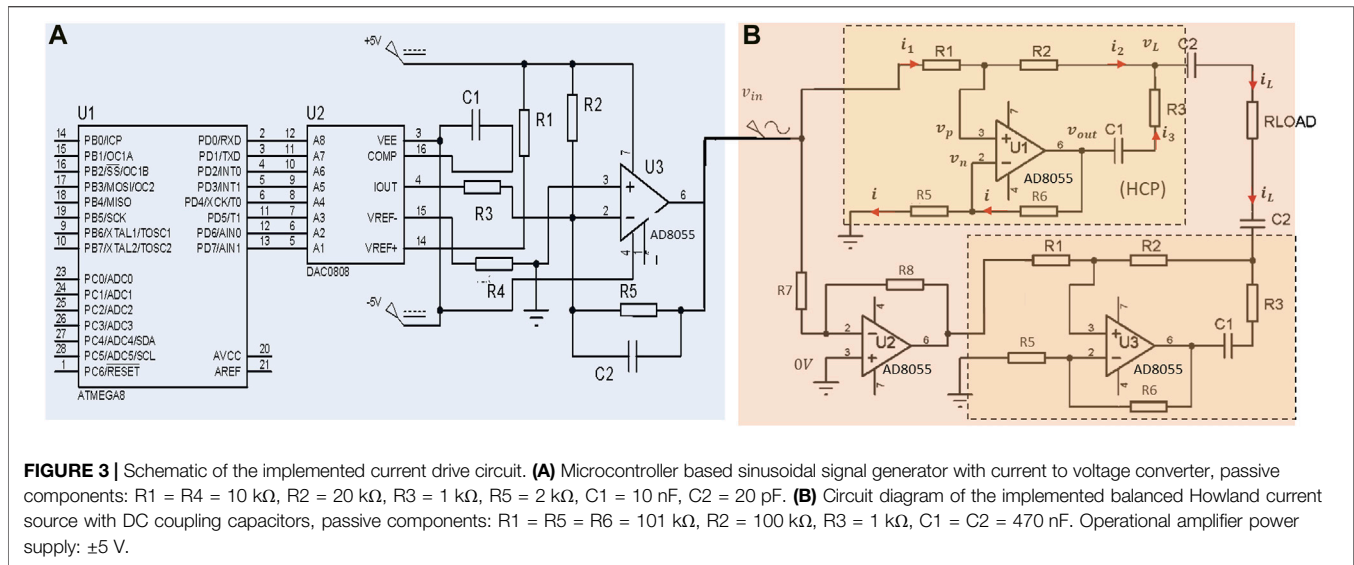
corresponding electrode tissue contact impedances, and this is expected to hold at all in-between frequencies. From both the background and this section, it can be seen that the output impedance of the current source is a key parameter in determining measurement accuracy and that the tissue impedance is much less than the electrode contact impedance. Using these, the output impedance of the current source for the FIM system was specified to be >200 k Ω at 10 kHz and >50 k Ω at 1 MHz; 100 times higher than the total driven impedance to give a measurement accuracy of 1%. The design requirements for the multi-frequency FIM system are summarized in **Table 1**.

System Design

An integral part of the system design was component selection. Since our aim was to have device that could be constructed, maintained and customized by researchers or their technical collaborators, we made a policy decision at the outset to only use through hole components, not surface mount devices (SMD). Hand construction and prototyping with the latter was deemed problematical unless specialist facilities were available. SMDs were designed to reduce the costs and size of mass-produced electronics, not for low-budget research developing novel instrumentation. We also wanted the design to be implementable in low resource settings and therefore we also required components to be widely available, including in these countries. Our criterion for determining whether or not to use a component was whether it was available through a major component supplier in Bangladesh where 2 of the authors (MAK and KSR) are based. Where the system specification could not be met with components that met the selection criteria, we chose components that were likely to meet it in the near future.

Our criteria for component selection impacted on the system design since it eliminated high speed micro-controllers, field





programmable gate arrays (FPGA) and digital signal processing devices. In particular it eliminated the use of digital demodulation techniques where multiple frequencies are applied to the tissue simultaneously (Wilson et al., 2001; Sanchez et al., 2012). Thus, the design was based on sequential measurements of the different frequencies. Options for analogue demodulation include full-wave rectification, techniques using analogue multiplication (e.g., multiplying the signal to be measured with a square wave), peak following and synchronous peak detection. With the exception of the synchronous peak detection technique, the other techniques all require time averaging of the detected peak values to give a dc voltage proportional to the amplitude. For an analogue implementation, the averaging is implemented as a low pass filter, typically a first order low pass filter, that gives an average with an exponentially mapped past. Thus, averaging occurs over long time periods limiting the ability of the instrument to measure small or rapid changes in impedance with time. Synchronous peak detection gives a cycle-by-cycle measurement of the amplitude and thus provide real-time information on impedance changes and this was the approach used in the FIM system described.

Figure 2 shows the block diagram of the multi-frequency FIM system where two microcontrollers were used. An analogue signal at the drive frequencies was generated using Microcontroller-1 with a digital to analogue converter (DAC), and a current to voltage converter. This voltage signal was then converted to a bipolar drive current using a balanced Howland current source circuit. The current drive was then applied to the target biological tissue through electrodes selected by multiplexers to give the appropriate FIM electrode configuration (see **Figure 1**).

The received voltage signal from the potential electrodes, selected using the FIM switching circuit, was amplified using a differential (instrumentation) amplifier (bioamp) and then passed through filters to reduce noise and unwanted signal components. The next requirement was to determine the peak

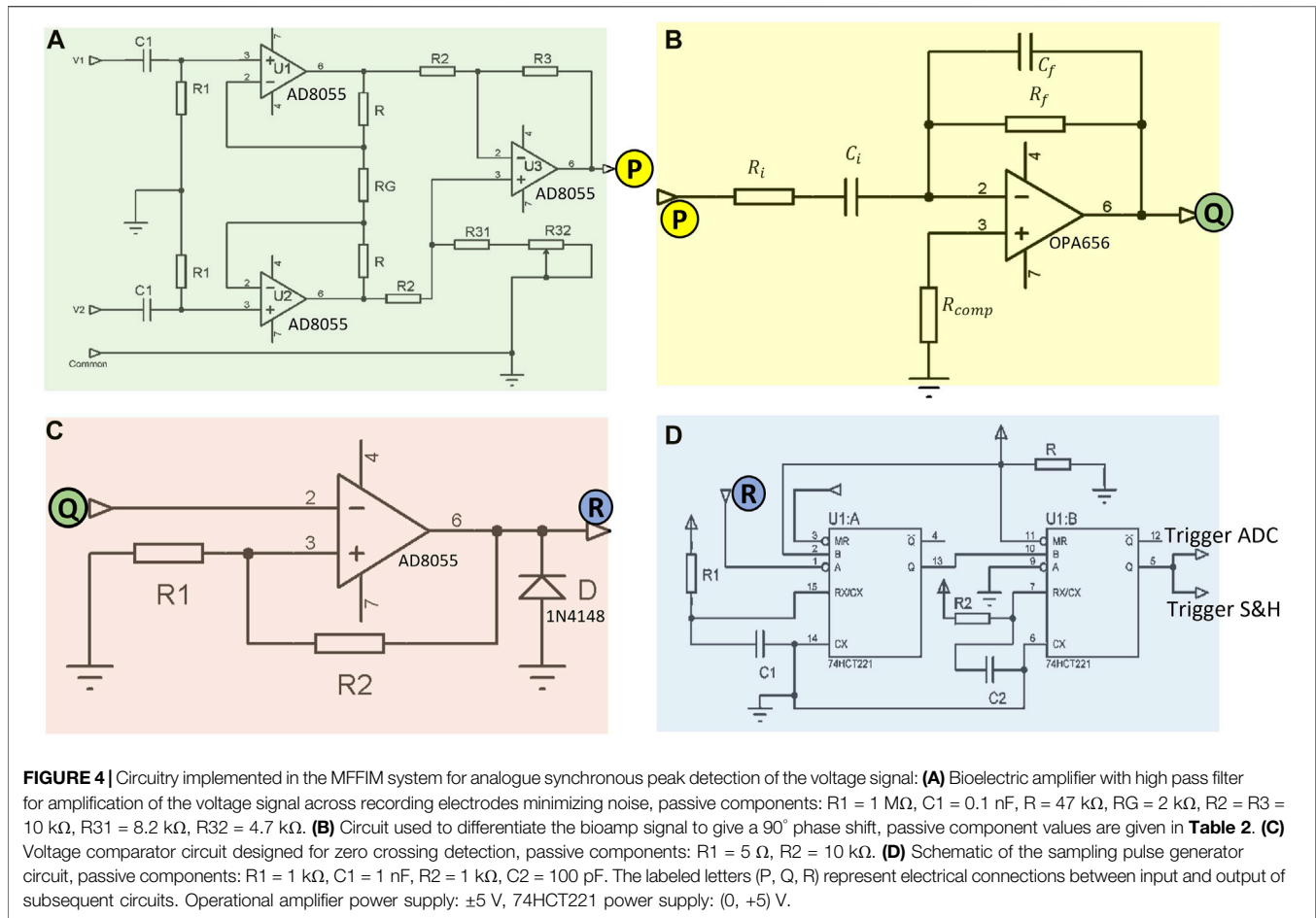
voltage of the output sinusoidal signal for which the rest of the circuit blocks in **Figure 2** were used. The scheme of this analogue peak detection method is explained in *Analog synchronous peak detection*.

Current Drive Circuit

For multi-frequency bioimpedance applications, the current drive circuit needs to set the excitation signal to different frequencies. A schematic of the current drive circuitry is shown in **Figure 3**. In the current drive circuitry of the designed MFFIM system, a microcontroller (Atmega8, Microcontroller-I in **Figure 2**) was used to generate sinusoidal waves as described in the following paragraph.

Signal Generator

Digital (8bit) amplitude values of samples from a full cycle of a sine wave were calculated and corresponding binary values were stored in the program memory of the microcontroller (U1 in **Figure 3A**). For digital-to-analogue conversion (DAC) the microcontroller (an Atmega8) used pulse-width-modulation requiring an external RC filter to produce the analogue voltage. Since different RC time constants would be needed for the different excitation frequencies, a separate digital to analogue converter (DAC0808) was used to generate the analogue drive signal. The 8 bit amplitude values (binary) were cyclically clocked through 8 I/O ports of the microcontroller to the DAC where the clocking rate determines the frequency of the output signal. The number of sample points is limited by the maximum clock rate (16 MHz), which equals the instruction rate of the microcontroller. Using 25 sample values per cycle with intervals of 14.4° and clocking these samples at 16 MHz resulted in a sinusoidal signal of 640 kHz. Signals of other lower frequencies were generated by reducing the clock frequency appropriately. Because of the limitation imposed by the maximum clocking speed of 16 MHz, a lower number of sample points per cycle, 15, was necessary for the generation of a



signal at 1 MHz. The DAC (0808) gives a current output which was fed to a current to voltage converter in which passive electronic components were chosen to obtain an output voltage of $\pm 0.5 \text{ V}$.

Constant Current Source

A balanced current source was chosen for injection of the sinusoidal signal of constant amplitude into the biological tissues. A bipolar modified *Howland current source* described by (Bertemes Filho, 2002) was used in the implemented MFFIM system as shown in **Figure 3B**. It is a combination of two identical modified *Howland current pumps (HCP)*. The input of the 2nd modified HCP was inverted so that the current sourced from the 1st modified HCP is totally sunked at the 2nd HCP. A unity gain inverting amplifier was used to feed the 2nd HCP ($R_7 = R_8 = 10 \text{ k}\Omega$).

The output current (considering peak amplitudes) through the load resistor R_{Load} is given by **Eq. 1**,

$$I_L = \frac{V_{in}}{Z_C} \quad (1)$$

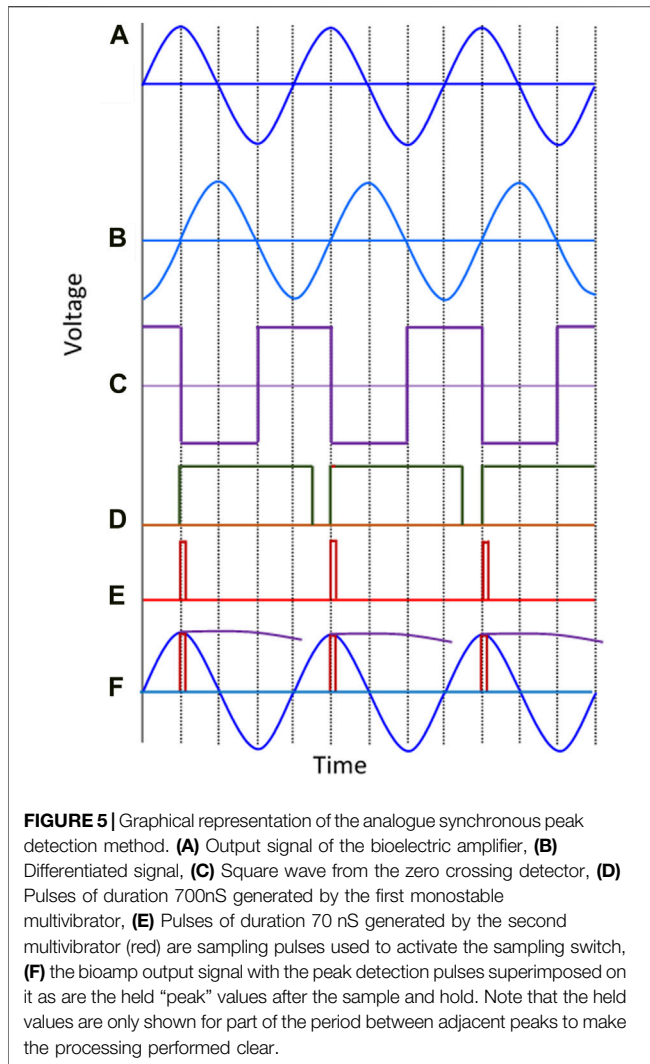
where V_{in} is the peak input voltage to the current source and $z_C = \sqrt{R_3^2 + X_{C1}^2}$ and $X_{C1} = 1/2\pi f C_1$.

Ideally, the current through the load is independent of the value of load resistance and depends only on Z_C , provided that

the ratio of resistors $\frac{R_2 + Z_C}{R_1} = \frac{R_6}{R_5}$. In practice, choosing appropriate electronic components (resistors, capacitors, and op-amps) is very important for a current source with high output impedance. So resistors of tolerance 1% (highest tolerance that met the component selection criteria) were used. The values of resistors and capacitors chosen for the implemented HCP circuit were $R_1 = R_5 = R_6 = 101 \text{ k}\Omega$, $R_2 = 100 \text{ k}\Omega$, $R_3 = 1 \text{ k}\Omega$ and $C_1 = C_2 = 470 \text{ nF}$. The value of R_3 was chosen to be $1 \text{ k}\Omega$ so that for an input signal of $V_{in} = \pm 0.5 \text{ V}$, the load current $I_L = \pm 0.5 \text{ mA}$. To maintain a high output impedance of the current source over the frequency range $10 \text{ kHz} - 1 \text{ MHz}$, fast, low power op-amps with a high gain bandwidth (GBW) product were required. The high-speed op-amp AD8055 with a CMRR, GBW and slew rate of 82 dB, 300 MHz, and $1400 \text{ V}/\mu\text{S}$ respectively was chosen for the implemented circuitry. Capacitors C_1 and C_2 were used to minimize op amp offset voltages and to prevent any dc signal to flow into the human body, which may cause harm.

Voltage Measurement Circuit

The voltage signal between the sensing electrode pair needs to be amplified minimizing the common mode potential on the body. A standard three-op-amp instrumentation amplifier circuit (Pallas-Areny and Webster, 1993) was used in the MFFIM



system (Figure 4A). Once again, the AD8055 (unity gain bandwidth: 300 MHz, slew rate: 1400 V/ μ S) was used. AC coupling at the inputs removes the dc contact potential and eliminates the possibility of the dc bias currents from the amplifiers reaching the body. The voltage sensing electrodes may also pick signals originating from myoelectric activities within the body, including those from the heart, but these are at a much lower frequency (0.01–100 Hz and 2 Hz–1 kHz, respectively) than the frequencies being measured (>10 kHz). Therefore, high pass filters with a cutoff frequency of 1,592 Hz were used, 5 times lower than the lowest frequency (10 kHz) being measured. The main source of the common mode voltage is capacitive coupling of the body to the 50 Hz mains power supply and can be up to 1,000 times larger than the common mode voltage produced by the injected current (Brown et al., 2017). To achieve high CMRR by matching resistor ratios, resistors of tolerance 1% were used in the implemented bioelectric amplifier. The resistors were chosen so that $\frac{R_3}{R_2} = (R_{31} + R_{32})/R_2 = 1$ nominally ($R_2 = R_3 = 10$ k Ω , $R_{31} = 4.7$ k Ω and $R_{32} = 8.2$ k Ω). A

multi-turn variable resistor R_{32} was used to trim the resistor ratios so that the common mode gain can be adjusted to a minimum. The gain of the differential amplifier section is unity and the values of resistors R and R_G were chosen to be 47 and 2 k Ω , respectively, so that the gain in the buffer amplifier stage is around 48.

The overall gain of the bioelectric amplifier was set to 48 so that the amplified signal voltage does not exceed the maximum op-amp output swing of ± 3.2 V with a power supply voltage of ± 5 V. If the transfer impedance to be measured is 100 Ω (maximum as specified) with an applied current amplitude of ± 0.5 mA, the voltage developed across the *receive* electrode pair equals ± 50 mV. With a gain of 48, amplified signal voltage amplitude is ± 2.4 V. So the maximum voltage amplitude to be acquired by the ADC is +2.4 V. The internal reference voltage (+2.56 V) of the Atmega8 ADC was used as reference.

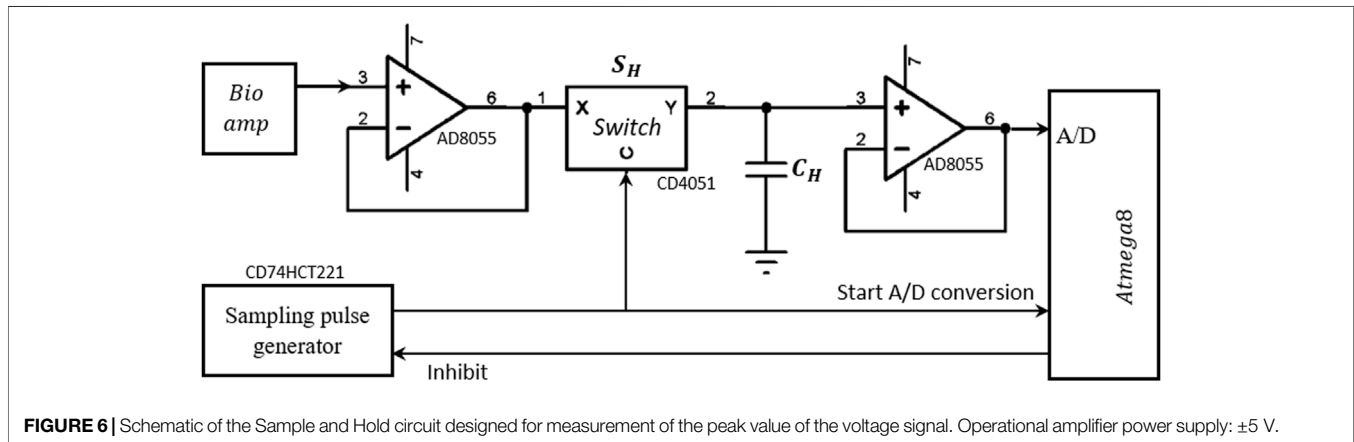
Analog Synchronous Peak Detection

Implementing synchronous peak detection was challenging for all the different circuit elements because of the wide dynamic range of frequencies it had to work over. The approach adopted was to have multiple phase detectors each of which covered a narrow frequency range. The principle, for each frequency, is illustrated in Figure 5. The signal from the bioelectric amplifier is first differentiated by passing it through an analogue differentiator, so there is a phase difference of 90° between the bioelectric amplifier output (Figure 5A) and the differentiator output (Figure 5B). The zero crossings of the differentiated signal (trailing edge of Figure 5C), correspond to the peak in the original signal which can be sampled by an appropriate pulse (Figure 5E) and held (Figure 5F). The blanking pulse (Figure 5D) prevents retriggering of the sample and hold process on noise.

A standard differentiator circuit (Figure 4B) was used for differentiating the bioamp output signal. An op-amp with high input impedance that was stable at low gains was required for this stage which has to operate over a wide frequency range. Therefore, an op-amp with JFET input (OPA656) was used. The output of the differentiator must be within the maximum output swing (± 3.2 V) of the op-amp as mentioned before. Since the maximum specified output of the bioamp was ± 2.5 V, the maximum gain of the differentiator circuit was chosen as 1.28. However, the output from the differentiator is proportional to the signal frequency. The designed signal frequency range is 10 kHz–1 MHz (a range of 1:100), therefore we should have a 100:1 dynamic range. Again, the *transfer impedance* range specified is 5–100 Ω , a 20:1 dynamic range. So the differentiator needs to work over a 2000:1 dynamic range (i.e., >60 dB). A single differentiator circuit to cover the required frequency range was not achievable, therefore, four different differentiator circuits with frequency dependent gain characteristics as shown in Table 2 were used. The differentiator circuits were switched according to the measurement frequency using a multiplexer. An analogue multiplexer (74HC4052), controlled by microcontroller-II, was used to select appropriate differentiators for specific choices of signal frequencies (not shown in the schematics).

TABLE 2 | Circuit parameters of four different differentiator circuits designed for various measurement frequencies.

Differentiator	R_i (Ω)	C_i (nF)	R_f (k Ω)	C_f (pF)	Measurement frequency (kHz)	Gain
I	100	1	10	10	10	0.628
II	100	1	2.2	10	20	1.256
					40	0.553
					80	1.104
III	20	1	0.56	10	160	0.563
					320	1.125
					640	0.802
IV	20	1	0.20	10	1024	1.276

**FIGURE 6** | Schematic of the Sample and Hold circuit designed for measurement of the peak value of the voltage signal. Operational amplifier power supply: ± 5 V.

The voltage comparator (**Figure 4C**) designed to detect zero crossing of the differentiator output which corresponds to the peaks of the target bioamp signal (**Figure 5A**). In order to stop output transitions because of the presence of noise a hysteresis was applied by feeding back a small fraction of the output voltage to the positive input. The reference voltage of the comparator designed was 0 V and hence its hysteresis can be expressed by **Eq. 2**:

$$V_{\text{hysteresis}} = \frac{R_1 (V_{OH} - V_{OL})}{R_1 + R_2} \quad (2)$$

where, V_{OH} and V_{OL} are the maximum and minimum output voltages (saturation voltages of the op amp), respectively. The values of resistors R_1 and R_2 were chosen as 5 Ω and 10 k Ω , respectively. For output voltages of ± 5 V, the thresholds of output transitions are ± 2.5 mV. The diode (1N4148) was used to prevent negative voltages at the input to multi-vibrator U1:A.

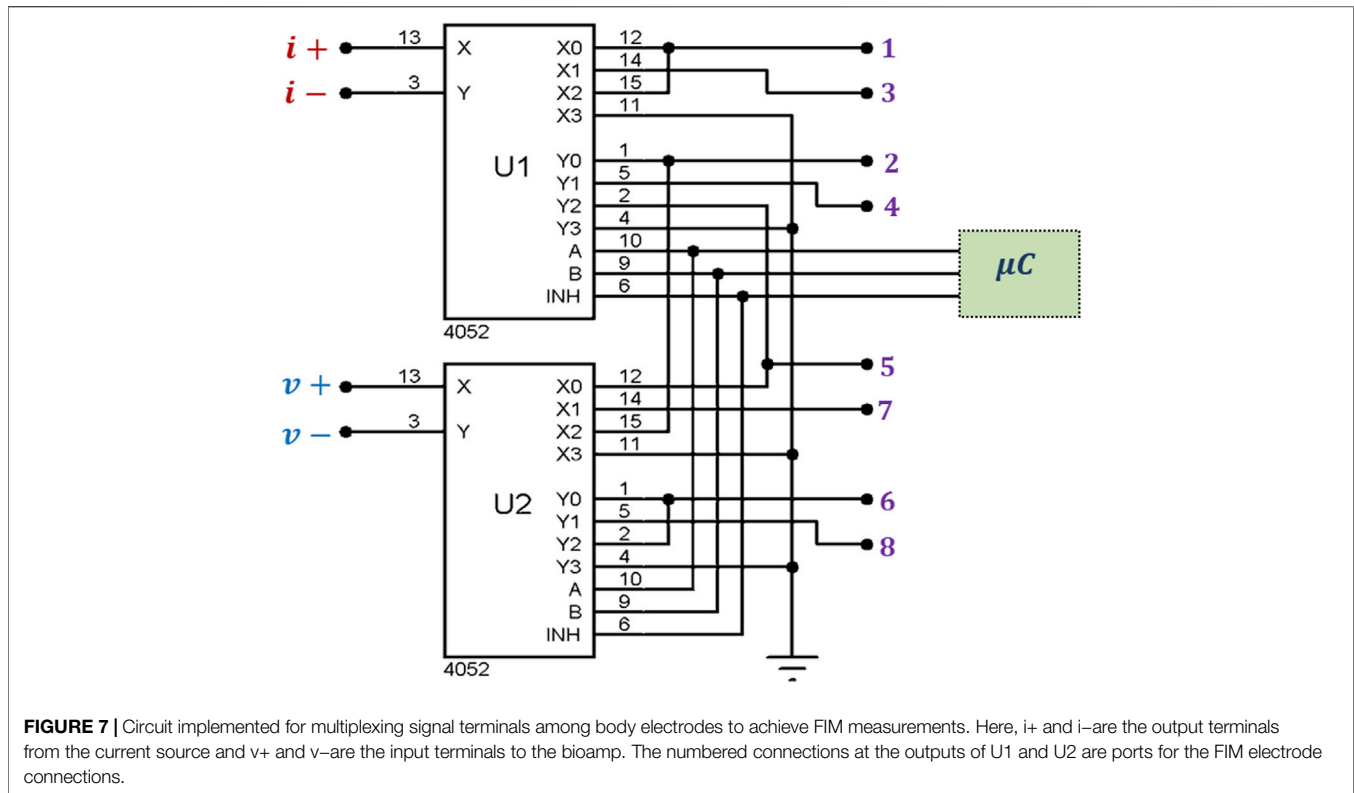
Sampling pulses (70 ns) were generated from a dual non-retriggerable monostable multivibrator (CD74HCT221) circuit (**Figure 4D**) that triggered a Sample and Hold (S&H) circuit, which in turn sampled the bioamp output signal at its peak. This value was then held stable for the conversion period (**Figure 5F**) of the analogue to digital converter (ADC) of Microcontroller-II.

Figure 6 shows the schematic of the S&H circuit implemented in the MFFIM system. A fast CMOS multiplexer CD4051 was used as the sampling switch. The time constant for charging the capacitor depends on the ON resistance (R_{ON}) of the switch and

on the capacitance (C_H). The typical value of R_{ON} for CD4051 is 80 Ω and the value of the hold capacitor was chosen to be 100 pF so that the charging time constant is 8 ns. The time duration of the sampling pulse (70 ns, as described in the previous section) is about 9 times longer than the charging time constant. Therefore the sampling pulse width is long enough to charge the capacitor at bioamp voltage level.

In the hold state, the switch is open; the capacitor C_H needs to hold the voltage value until the A/D conversion is complete. But in practice, the capacitor is discharged through both the input resistance (R_{in}) of the buffer amplifier and as a result of the bias current flowing into the amplifier. The input bias current of the op-amp (AD8055) used in the buffer amplifier is 1.2 μ A. Typically, the A/D conversion of the microcontroller (Atmega8) needs 13.5 μ s; and during this period the hold capacitor discharges only 1.34% of its initial value for a 1.2 V input signal which is practically acceptable.

The rising edge of the sampling pulse of the S&H circuit was also used as an interrupt pulse which initiates the A/D conversion of the microcontroller-II. There is an internal 2 clock pulse delay between triggering the interrupt and initiation of the conversion process during which the ADC was initialized. Therefore, no extra delay was necessary between the sampling pulse of the S&H circuit and that to trigger the ADC circuit enabling the same pulse to trigger both. The ADC of the Atmega8 microcontroller requires 13.5 μ s for each conversion. For measurement frequencies greater than 80 kHz, the time period between two



successive peaks is $<13.5 \mu\text{s}$, therefore, subsequent trigger pulses could be generated from the sampling pulse generator before the ADC conversion of the previous sample is complete. To prevent this, the monostable multivibrator output was gated (inhibited) by programming microcontroller-II so that it cannot initiate further sampling pulses before completion of the current ADC conversion. The overall gain of the voltage measurement circuit based on analogue synchronous peak detection was set to 48. Therefore for a drive current of 0.5 mA peak and transfer impedance of 100Ω , the peak voltage across the receive electrode pair is 50 mV before amplification. After 48 times amplification, the voltage peak should be 2.4 V. The resolution of the ADC of the voltage measurement microcontroller is 10 bit with reference voltage 2.56 V. Therefore, the measurement resolution for the synchronous peak detection method is 0.1Ω .

FIM Switching

From **Figure 1** it can be seen that there are 3 versions of the FIM electrode configurations, i.e., FIM-8, FIM-6 and FIM-4. The Focused Impedance Method requires two tetrapolar (TP) measurements at each frequency where the direction of current drive and voltage measuring electrode pairs are altered orthogonally as summarized in **Figure 1**. This section describes the FIM switching mechanism implemented (**Figure 7**). There are four signal terminals; two for current drive ($i+$ and $i-$) and two for voltage measurement ($v+$ and $v-$) for each TP measurement. FIM measurements were achieved by switching the current and voltage signals to appropriate electrodes for a

particular FIM configuration. For this purpose, up to eight connectors to these electrode ports (denoted:1-8) could be fitted to the device; the exact number being dependent on the FIM configuration and application area being investigated. These ports were used for the electrical connections to the electrodes. Analog multiplexers (CD4052) were used to establish electrical conduction path among *signal terminals* and electrode ports (**Figure 7**) appropriate for a particular FIM configuration as described in **Figure 1**. The multiplexers were controlled from the microcontroller using I/O terminals.

For the FIM-8 configuration, all the eight ports (1-8) need to be used and the two TP orthogonal measurements were performed by switching *signal terminals* among body electrodes sequentially according to **Table 3**. In this scheme, measurement-I is performed by connecting *signals terminals* to the electrode ports 1,2,5,6 and then Measurement-II is performed by connecting *signal terminals* to the ports 3,4,7,8; which in turn connect *signal terminals* to the electrodes A,B,C,D and E,F,G,H, respectively. The microcontroller is programmed so that it records voltage signal from horizontal electrodes; and then changes the multiplexer control inputs to record the signal for vertical electrodes of **Figure 1** at each measurement frequency.

In the FIM-6 configuration, the electrode ports 7 and 8 are not used; only the *current* terminals are switched while voltage signal is recorded from the same electrode pair (K,N). In the FIM-4 configuration, only four ports (1,2,5, and 6) need to be used. In this case, only the signal terminals $i-$ and $v+$ are switched between the electrodes L and M (ports 2 and 5) to achieve the

TABLE 3 | Switching sequences for different FIM measurements. Multiplexers are controlled by a microcontroller to establish electrical conducting path between signal terminals and body electrodes for FIM measurements.

Electrode Configuration	Measurement sequence	Multiplexer control input			Multiplexer ON channel	Electrical connection pathway		
		Multi-plexer	B	A		Circuit terminal	Port no	Body electrode
FIM-8	I	U1	0	0	X-X ₀	i+	1	A
					Y-Y ₀	i-	2	D
		U2	0	0	X-X ₀	v+	5	B
	II				Y-Y ₀	v-	6	C
		U1	0	1	X-X ₁	i+	3	E
					Y-Y ₁	i-	4	H
FIM-6	I	U1	0	0	X-X ₀	i+	1	A
					Y-Y ₀	i-	2	D
		U2	0	0	X-X ₀	v+	5	K
	II				Y-Y ₀	v-	6	N
		U1	0	1	X-X ₁	i+	3	E
					Y-Y ₁	i-	4	H
FIM-4	I	U1	0	0	X-X ₀	i+	1	K
					Y-Y ₀	i-	2	L
		U2	0	0	X-X ₀	v+	5	M
	II				Y-Y ₀	v-	6	N
		U1	1	0	X-X ₂	i+	1	K
					Y-Y ₂	v+	2	L
				X-X ₂	i-	5	M	
				Y-Y ₂	v-	6	N	

FIM measurements. Impedance measurements for all of the three FIM configurations can be performed using the designed multi-frequency FIM system as explained in **Table 3**.

Data Acquisition

The Universal Synchronous and Asynchronous Serial Receiver and Transmitter (USART) peripheral of the ATmega8 microcontroller was used to communicate with a personal computer that was employed to process and store the measured data. A serial to USB adaptor (TTL232-5 V) was used to connect the FIM system to the commonly available USB port of a PC. An open source terminal program “RealTerm” was used to acquire and store data on PC.

Microcontroller-II acquired 10 consecutive peak values of the bioamp output through ADC conversion for a TPIM measurement at a particular frequency which were then averaged them before sending the resultant value to the PC via the serial link. Another TPIM measurement is then performed at the same frequency by changing the drive and receive electrode pairs through FIM switching algorithm and then sent to the PC. The sequence was then repeated for the other measurement frequencies. Focused impedance values were obtained by averaging the two TPIM values from each measurement frequency in the PC.

Isolation and Safety

To ensure patient safety all patient connections on electro-medical equipment should be electrically isolated from the mains supply. The multi-frequency FIM system described in

this paper required a total current of approximately ± 100 mA from a ± 5 V supply. The need for electrode switching under microprocessor control means that the voltage measurement and current source sections cannot be easily isolated from the other parts of the system. Therefore the whole measurement system is powered from a medical grade isolated power supply (THB 3-1,222 manufactured by TRACO® POWER) that satisfies the IEC/EN 60601-1 safety standards (IEC, 2004) for patient connected electro-medical equipment. The output of the power supply is ± 7 V which was converted to ± 5 V using regulators. The power supply can isolate up to 5 kV.

For storage and analysis of data, the device is connected to a PC which may be connected to mains supply. Isolation between the data acquisition system and the PC was achieved using high speed *opto-couplers* (HCPL 2531) on the serial data lines (Rx, Tx) connecting the two. The isolation measures taken for patient safety are illustrated in **Figure 8**. In addition, all electrode connections to the patient were ac coupled using capacitors to prevent any dc currents passing to the patient, which are associated with hazards.

PERFORMANCE ANALYSIS

Signal Frequency

The microcontroller based signal generator of the MFFIM was designed to generate sinusoidal signals of frequencies: 10, 20, 40,

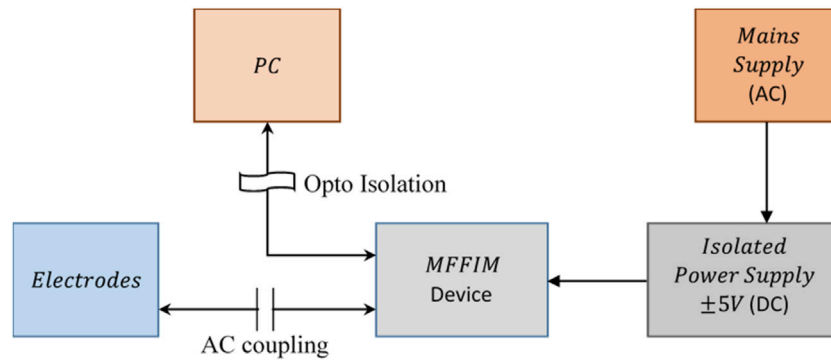


FIGURE 8 | Isolation of the measurement device from mains supply to ensure patient safety. The power is taken from a medical grade isolated dc power supply while the communication with PC is optically coupled for the device based on analogue synchronous peak detection.

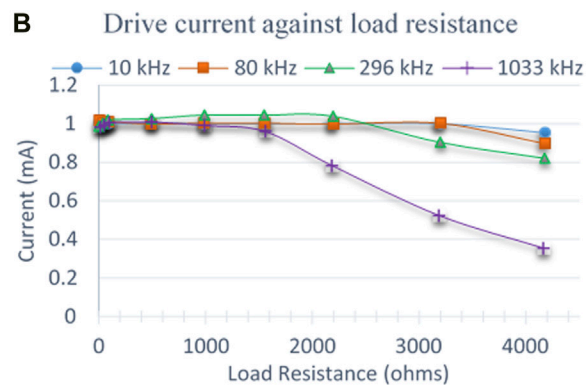
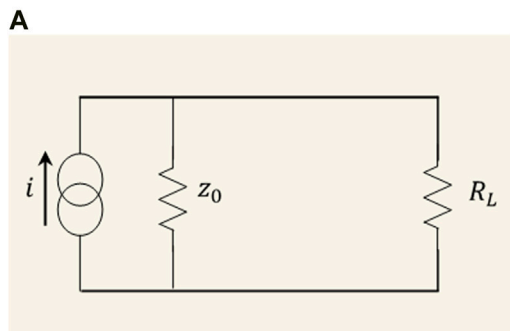


FIGURE 9 | (A) Equivalent circuit used to model the output impedance of the current source (B) Drive current plotted against load resistances at four representative frequencies.

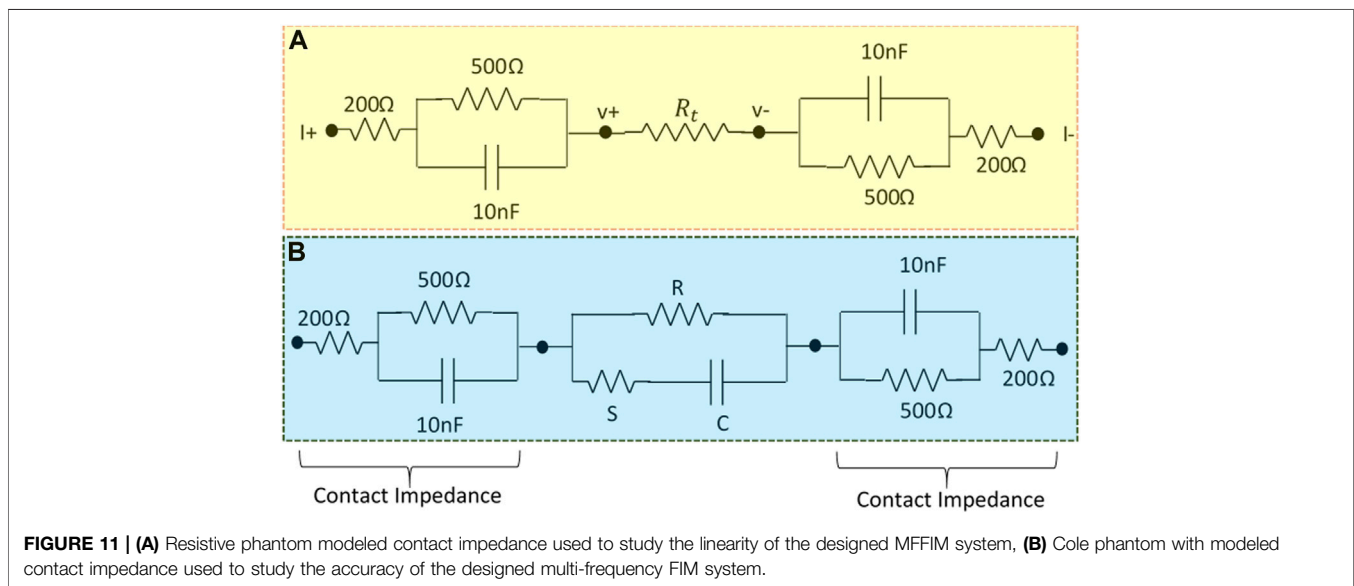
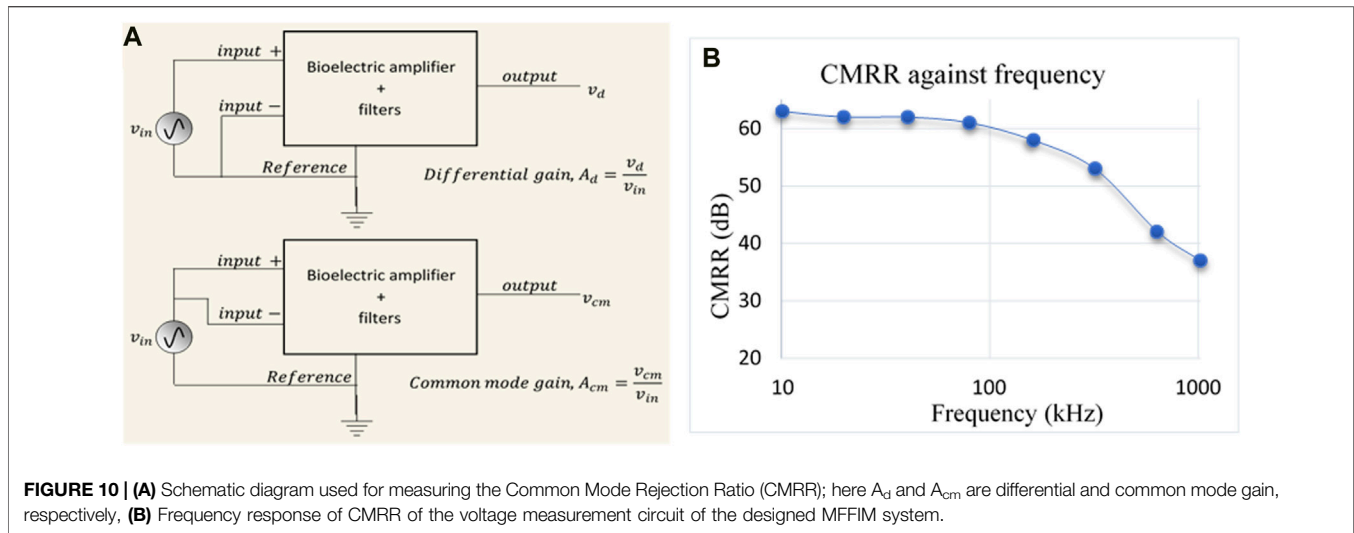
80, 160, 320, 640, and 1,024 kHz. However, the actual frequencies of the signals generated by the implemented circuit were measured using a calibrated oscilloscope and found to be 10, 20, 40, 80, 160, 296, 633, and 1,033 kHz, respectively, (rounded to the nearest kHz). The generated signal frequencies are close to the frequencies specified except signals at high frequencies, particularly at 296 kHz which is 24 kHz lower than that specified. The frequency at which the binary sample values are clocked out for these high frequencies were obtained by dividing the processor clock frequency. For the Atmega8, the processor clock frequency is the same as the instruction execution rate, so there may be some delays within the microcontroller for the program counter and interrupt service checks. The time lag, which is negligible at low frequencies, may be the reason for the differences in the top two frequencies where 25 point sampling was used. However, the differences are small and the resultant values are acceptable since it is the variation of transfer impedance with frequency that is intended to be analysed in the studies. Total harmonic distortions (THD) of the generated sinewaves were found to be 0.167% at 10–633 kHz and 0.33% at 1,033 kHz.

Current Source Output Impedance

The current source can be modelled as a constant current generator in parallel with a resistance (output impedance). To measure the output impedance (Z_O) of the current drive circuit, two different load resistances (R_L) were driven by the current at each frequency (Figure 9A). If V_1 and V_2 were the voltage developed across $R_L = R_1$ and $R_L = R_2$, respectively, then:

$$z_0 = \frac{(V_2 - V_1)R_1R_2}{(V_1R_2 - V_2R_1)} \quad (3)$$

The output impedance (Z_O) was calculated using Eq. 3 by measuring the voltages across two different load resistors 97.8 and 991 Ω (these were the measured resistance values using a calibration checked multi-meter for standard resistors 100 and 1,000 Ω , respectively). Thus the output impedance of the current source was found out to be 476 k Ω at 10 kHz and 58.3 k Ω at 1,033 kHz, respectively. The current source was designed to deliver peak currents of ± 0.5 mA to load resistances up to 4 k Ω . Figure 9B shows the drive current against load resistances at different frequencies. The drive current is almost constant up to a load of 3 k Ω for signals up to 80 kHz but starts to



drop above this. For 296 kHz signal, the current drops above a load of 2 k Ω while for 1,033 kHz signal, the drive current drops above 1.5 k Ω . It should be noted that these measurements are for the current source without connection to the multiplexers that select the drive and receive electrodes.

Common Mode Rejection Ratio

For an ideal op-amp the Common Mode Rejection Ratio (CMRR) of the differential amplifiers used in the MFFIM system is determined by the matching of the resistors in the differential element. However, the presence of series impedances and stray capacitances degrade the CMRR of the overall circuit. The CMRR of the voltage measurement circuit of the designed MFFIM was obtained experimentally at all the eight measurement frequencies. The differential mode gain (A_d) and the common mode gain A_{cm} was measured feeding sinusoidal signals from a standard signal

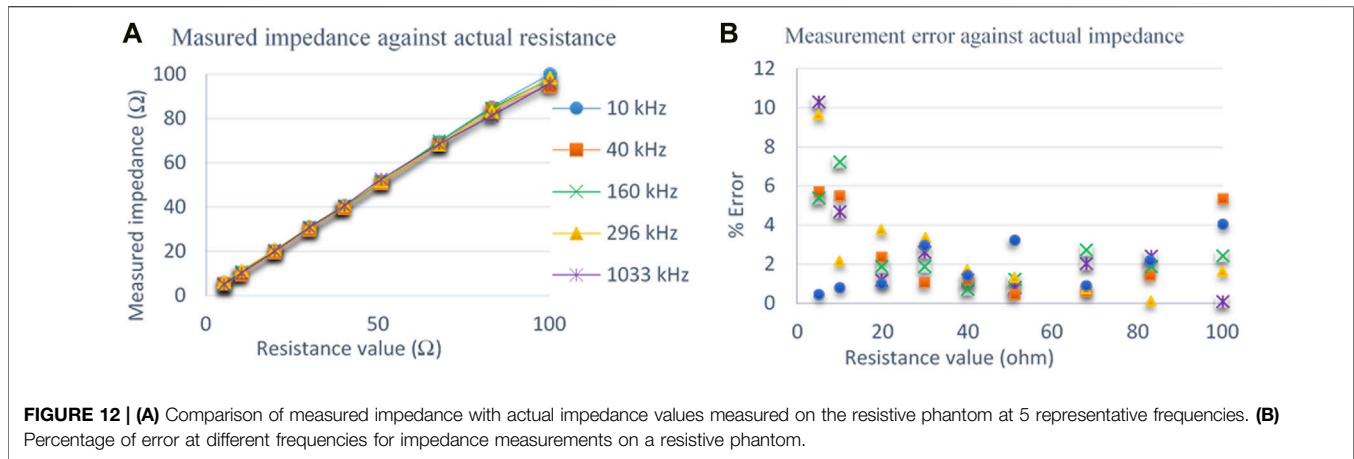
generator as illustrated in **Figure 10A**. These measurements included the input high pass filters of the voltage measurement circuit. CMRR was then calculated using **Eq. 4**:

$$CMRR = 20 \log \left(\frac{A_d}{A_{cm}} \right) \quad (4)$$

Experimental values of CMRR were plotted against frequency in **Figure 10B**. It can be observed that the value of CMRR was 63 dB at 10 kHz and remains above 60 dB up to 100 kHz beyond which it decreases and reduced to 37 dB at 1,024 kHz.

Linearity and Measurement Accuracy in Resistive Phantom

To study the accuracy and linearity of the developed instrument, transfer impedance values were measured on a passive circuit



phantom as shown in **Figure 11A**, where R_t represents the target tissue impedance (here resistive) to be measured while the RC network on both sides represent the electrode-tissue contact impedance. Electrode-tissue contact impedance was considered to be $1.4 \text{ k}\Omega$ at 10 kHz , 700Ω at 100 kHz , and 430Ω at 1 MHz from which the resistor and capacitor values shown in **Figure 11** were calculated. The current drive terminals, taken from the output terminals of the multiplexers, in the developed MFFIM system were connected to the two ends of this network while the potential terminals were connected across R_t . Essentially, it measures TPIM or four electrode impedance on this passive circuit phantom. Different values of R_t were used for this study. These values of R_t were measured using a calibration-checked digital multi-meter initially to serve as the reference values. The designed multi-frequency FIM system was then used to perform four electrode impedance measurements on the RC phantom employing the analogue peak detection techniques. The values of R_t was varied within the measurable transfer impedance range mentioned before.

Figure 12A shows the measured impedance values of R_t using analogue synchronous peak detection method against the directly measured reference values of R_t . It can be observed that the measurements agree very well for all frequencies and for the range of resistance values used for R_t . Of course, there is a slight nonlinearity at $1,033 \text{ kHz}$ but it is not much.

For the above measurements on resistive phantoms, the accuracy of measurements were determined. If the applied known resistance was R_{known} and the resistance measured by the multi-frequency FIM system was R_{measured} , then the percentage of error (absolute value) was calculated using **Eq. 5**.

$$\text{Error} = \frac{|R_{\text{actual}} - R_{\text{measured}}|}{R_{\text{actual}}} \times 100\% \quad (5)$$

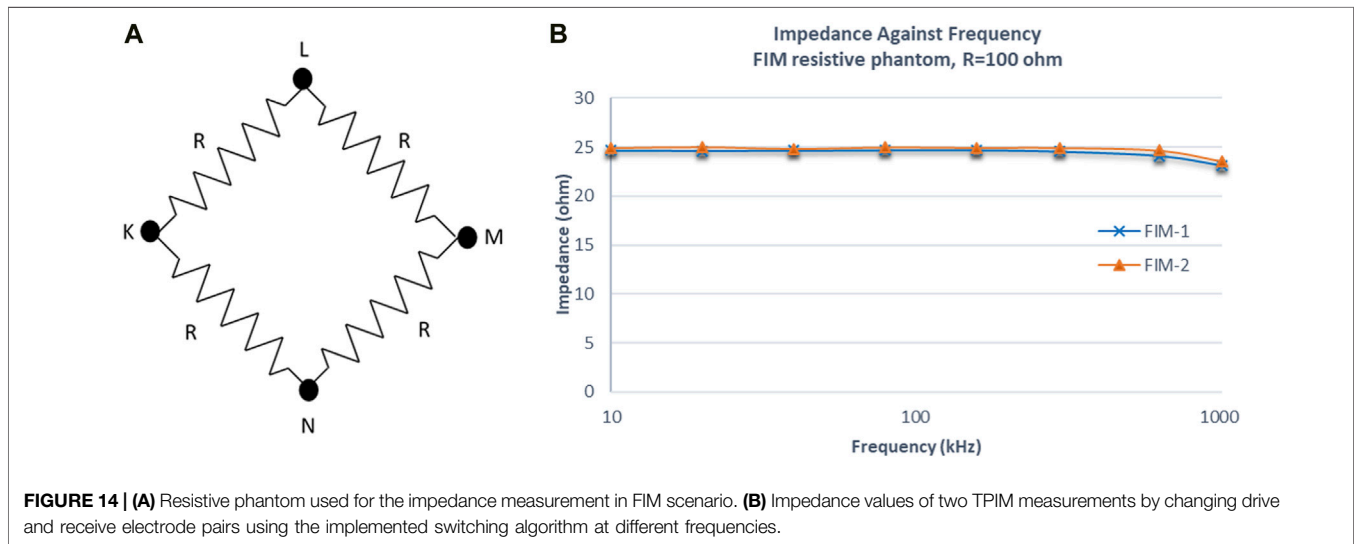
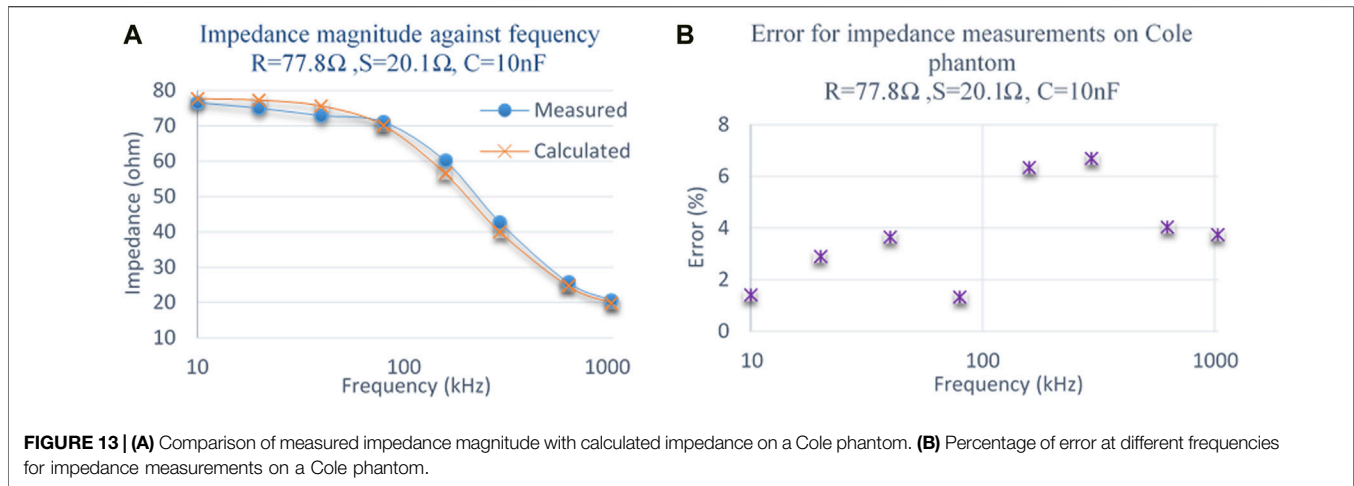
Figure 12B shows the percentage of measurement error against actual resistance values of R_t at the five measurement frequencies. It can be seen that from 20 to 100Ω , the errors are 4% or less except for 100Ω at 40 kHz , but which is still below 6% . Only for values at low resistances ($\leq 10 \Omega$) the errors are higher, going to about 10% for 5Ω .

Measurement Accuracy in Resistive-Capacitive Phantom (Cole Model)

The complete multi-frequency FIM system was also tested for complex loads as encountered in biological systems by replacing the load resistor R_t with a Cole-Cole model phantom as shown in **Figure 11B** where C represents membrane capacitance, R represents extra cellular resistance and S represents intra cellular resistance. The resistor-capacitor model on both side of the Cole-Cole model is to simulate contact impedances as before. The impedance values measured using the developed FIM system employing the analogue synchronous peak detection technique for this Cole-Cole model ($R = 77.8 \Omega$, $S = 20.1 \Omega$ and $C = 10 \text{ nF}$) is plotted against calculated impedance values in **Figure 13A**. As mentioned before, impedance values measured on human chest and breast using typical electrode configurations vary from 5 to 50Ω in the frequency range 10 kHz to 1 MHz (Al Amin et al., 2014; Kadir et al., 2015). So the values of the Cole model components were chosen to represent similar transfer impedance values in the measurement frequency range. Analysing the errors between the measured and calculated impedance values for this phantom showed that the maximum error was around 6.7% at signal frequencies 160 and 296 kHz whereas the error at other frequencies was below 4% as shown in **Figure 13B**. It can be noted that the errors are randomly distributed over the measured frequency range. This indicates that the approach of using separate differentiators in different frequency range were working correctly.

Measurement in FIM Scenario

One of the major purposes of the multi-frequency FIM system was to perform two orthogonal TPIM measurements at each frequency by switching the drive and receive electrode pairs automatically. To test this switching performance, measurements were taken by the developed multi-frequency FIM on a resistive phantom shown in **Figure 14A**. For one set of FIM measurement (FIM-1) the current drive terminals of



MFFIM instrument $i+$ and $i-$ (Figure 7) were connected to phantom terminals K and L , respectively, and the potential measuring (receive) terminals of the MFFIM instrument $v+$ and $v-$ were connected to the phantom terminals M and N respectively. For an orthogonal test (FIM-2) the current drive points were K and N while the potential measuring points were M and L , respectively; the switching between points was performed by the MFFIM device automatically. Figure 14B shows the results of these two orthogonal TPIM measurements for $R = 100\ \Omega$ which we call FIM-1 and FIM-2, respectively.

The current I applied (0.5 mA) between terminal K and L will flow through two paths: $K-L$ and $K-N-M-L$. Since the values of all the resistors are same ($R = 100\ \Omega$), the current through path $K-N-M-L$ will be one fourth of the applied current. Therefore, the voltage V across $M-L$ would be $25*I (=100*I/4)$ and theoretically the expected transfer impedance, V/I would give a value of $25\ \Omega$. It can be seen that the measured values follows the theoretical value closely at all frequencies.

DISCUSSION

The prototype FIM system developed allows bioimpedance measurements selecting a particular FIM configuration at multiple frequencies under software control from a PC. Figure 15 shows the PCB with fabricated electronic components and the front panel as well as the back panel of a prototype MFFIM system. Characteristics of the implemented multi-frequency FIM system are summarized in Table 4. The multi-frequency FIM system developed has potential application in a number of areas where bioimpedance measurements are used including the diagnosis of lung disorders and breast malignancy. The output impedance of the current generator was $476\text{ k}\Omega$ at 10 kHz , decreasing to $58.3\text{ k}\Omega$ at 1 MHz . These values exceed the design specification for 1% measurement accuracy discussed in Design Considerations, i.e., $>200\text{ k}\Omega$ at 10 kHz and $>50\text{ k}\Omega$ at 1 MHz . Whilst these meet the design specification, we acknowledge that the higher frequency value is low and the measurement was made without the multiplexers. However,

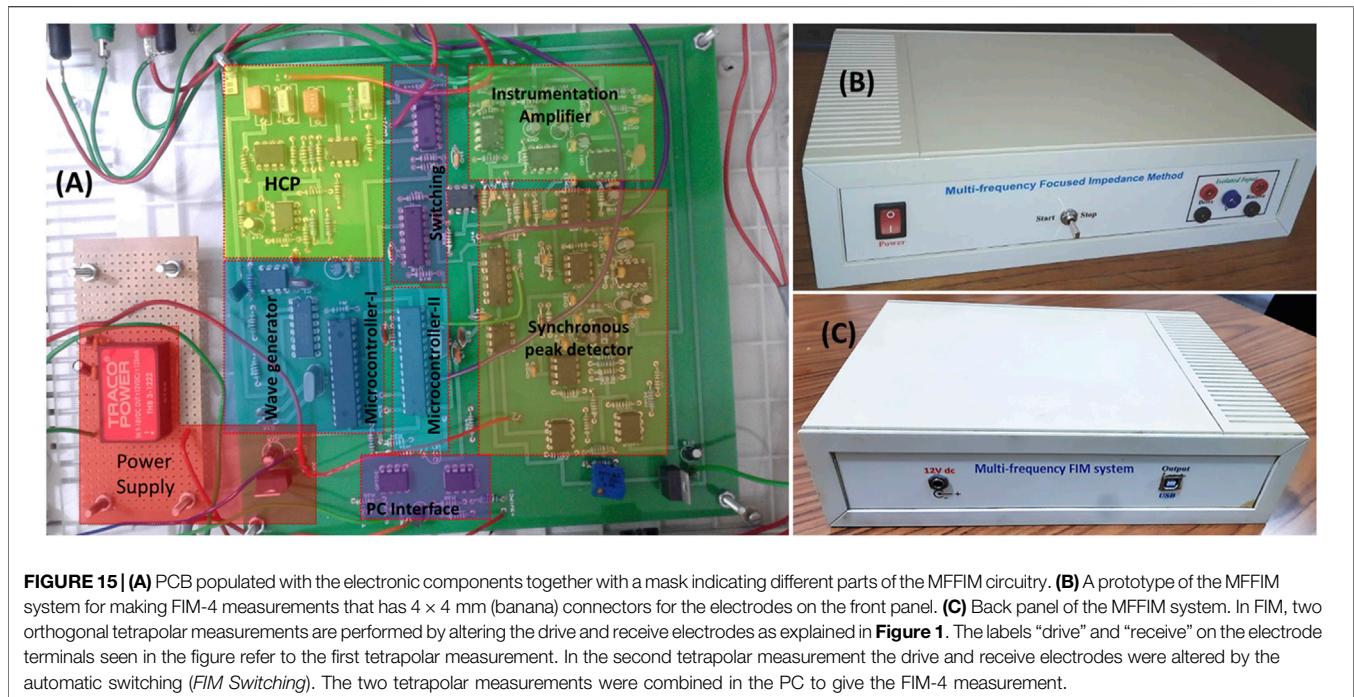


FIGURE 15 | (A) PCB populated with the electronic components together with a mask indicating different parts of the MFFIM circuitry. (B) A prototype of the MFFIM system for making FIM-4 measurements that has 4 × 4 mm (banana) connectors for the electrodes on the front panel. (C) Back panel of the MFFIM system. In FIM, two orthogonal tetrapolar measurements are performed by altering the drive and receive electrodes as explained in **Figure 1**. The labels “drive” and “receive” on the electrode terminals seen in the figure refer to the first tetrapolar measurement. In the second tetrapolar measurement the drive and receive electrodes were altered by the automatic switching (*FIM Switching*). The two tetrapolar measurements were combined in the PC to give the FIM-4 measurement.

TABLE 4 | Characteristics of the implemented multi-frequency FIM system.

Feature	
Frequency range	10 kHz-1 MHz
Current amplitude	0.5 mA
Current source output impedance	476 k Ω at 10 kHz and 58.3 k Ω at 1 MHz
THD	$\leq 0.33\%$
CMRR	63 dB at 10 kHz and 37 dB at 1 MHz
Impedance resolution	0.1 Ω
Impedance measurement error	<6%
Frame rate	45
Dimension	30 cm × 20 cm × 7 cm
Power consumption	500 mW

the value of 500 Ω used for the electrode contact impedance was conservative and values below 200 Ω have been reported at 1 MHz (Nguyen et al., 2013; Yang et al., 2017). We note that the value obtained is consistent with values reported for modelled current sources without multiplexers (e.g. Bertemes-Filho et al., 2012). An improvement in the output impedance of the current generator at the higher frequencies can be achieved by using resistors of tolerance better than 1% and higher frequency op-amps (Bertemes-Filho et al., 2012; Bertemes-Filho et al., 2016). Additionally, measurement of injected current amplitude can increase the impedance measurement accuracy and that may be implemented in future designs. The total harmonic distortions of 0.167% at 10–633 kHz and 0.33% at 1,033 kHz are comparable to that of the systems developed for similar application (Castro et al., 2016).

For epithelial tissue measurements inside body orifices and cavities the electrodes will be smaller and closer together (e.g. Abdul et al., 2006) and the drive current will need to be reduced to

microampere range to prevent local tissue heating due to the high current density. For such applications the analogue circuitry has to be redesigned and evaluated but the same switching circuitry can be used.

It should be noted that FIM measures the impedance amplitude, but no phase measurement is possible. There are well recognised problems in measuring and interpreting the phase from transfer impedance measurements. The position is even more complex for FIM which is the sum of two spatially separated transfer impedance measurements where the contributions from different parts of the volume under interrogation will be different for the two measurements. As a result, we view FIM as a magnitude measurement technique with the phase having no physical meaning.

The Common Mode Rejection Ratio (CMRR) of the bioelectric amplifier used to amplify the voltage signal was 63 dB and 37 dB at 10 and 1,024 kHz, respectively, (**Figure 10B**). Since any amplification of the common mode signal resulting from injected current gives rise to a measurement error, amplifiers used in impedance measurement systems require a high CMRR at the measurement frequency. In the context of EIT systems, it has been suggested 66 dB is required for 0.1% accuracy (Rossell and Riu, 1992) and that up to 72 dB is required depending on the position of the reference electrode. Achieving a high CMRR at high frequencies is challenging due to stray capacitances. Increasing the current value of 37 dB, which includes connecting cables, is an area for consideration when seeking to improve the overall accuracy of the system. A CMRR of 90 dB at 2 MHz has been reported in custom designed components for on-chip fabrication where connecting cables can be minimised (Worapishet et al., 2010). However, such an approach is not appropriate for a discrete component based system constructed from widely available components.

For the voltage measurement circuit based on analogue synchronous peak detection, the overall gain of the bioelectric amplifier was set to 48. The output voltage of the bioamp could not be greater than 5 V (peak-to-peak) in order to avoid exceeding the input voltage range of the ADC in the microcontroller. On the other hand, if the bioamp output was less than 250 mV, the output of the differentiator at 10 kHz would be too small to be detected by the voltage comparator. Taking the gain to be approximately 50, the measurable input voltage range for the measurement section was 5mV–100 mV (peak to peak). Therefore, with the excitation current of 1 mA (peak to peak) the measurable range for transfer impedance range is 5–100 Ω , a dynamic range of 1:20. Brown et al. (1994) reported that transfer impedance in the thorax region for signal frequencies 9.6–614.4 kHz lies between 14 and 25 Ω . In another study the impedance associated with alveolar edema was found to be 35% below an initial impedance value of 21 Ω (Fein et al., 1979). According to Al Amin et al. the transfer impedance in the breast tissue varies from 10 to 60 Ω in the frequency range 5–200 kHz (Al Amin et al., 2014). Therefore the transfer impedance range of the designed multi-frequency FIM system is adequate for impedance measurements in thorax or breast tissues. However, the gain of the voltage measurement circuit could be adjusted to investigate tissues having other impedance ranges. Although not currently implemented, a switched gain with the gain controlled from microcontroller could be implemented. As the switching would be under microprocessor control and the amplifier output was digitized/acquired by the same microprocessor, it would be possible to implement an automatic gain control.

The output impedance of the current source was measured without connection to the multiplexers used to select the drive and receive electrodes. Using multiplexers to select electrodes is a problem in all multi-measurement impedance instrumentation including EIT systems (Holder, 2004). From the data sheet, the input capacitance of the multiplexers used was typically 5pF and this limits the output impedance of the current source at the highest two frequencies, and ultimately limits it at frequencies much higher than those used by the system described in this paper. To put this into context: 5 pf at 1 MHz has reactance of 32 k Ω ; this in parallel with the 58 k Ω output impedance of the current source without the switching gives an effective current source output impedance driving the tissue of 21 k Ω at 1MHz, limiting the impedance the current source can drive to 200 Ω for 1% measurement accuracy. In practice, the impact on the measurement accuracy is small as the electrode contact impedance and the tissue impedance all decrease with increasing frequency. The only solutions are to measure the current driven into the tissue or to use a multi-channel approach with pairs of electrodes having their own current source and bioamp (e.g. Wilson et al., 2001). A recent development of the former approach has shown that using the measured current to control the output current from the current source gives a current source with a high output impedance when multiplexers are used (Sirtoli et al., 2019). All these approaches have substantial cost and complexity

implications but should be considered as part of future developments.

We breached our component selection criteria on a number of occasions; in particular, the lack of availability of high-speed op-amps in low resource settings presented a substantial problem as the design specification could not be achieved without them. The AD8055 and OPA656 did not meet our component selection criteria. However, at the time the work was done, they were widely used in general electronic instrumentation and lower specification op-amps from the same manufacturer did meet the criteria. There was therefore a reasonable probability that they would become available in the near future. The microcontroller (Atmega8) used in this design can execute one instruction in one clock cycle and was the most powerful available that met our component selection criteria. The amount of processing and control that needed to be delivered meant a single Atmega8 could not be used for both for signal generation and data acquisition/switching control. Moreover, the number of pins available on a single microcontroller was not sufficient for all the interfacing. Therefore, two separate microcontrollers were used in the implemented system. The medical grade isolated power supply was used for convenience, but an equivalent could be made out of discrete components that met our component selection criteria. The inclusion of surface mount devices (SMDs) in our component selection criteria would not have greatly extended the components available to us at the time the work was done. The decreasing availability of through hole devices and the increasing range of microcontrollers available means that in the future this restriction may not be appropriate. Since this work was finished, cheap, high performance single board microcontroller systems have come on the market, primarily intended for use by recreational programmers (hobbyists) (e.g., Teensy; www.pjrc.com). In our opinion it is only a matter of time before these become available in low resource settings and they provide an easily programmable building block with the potential to move the signal processing from hardware to software without the need for hardware construction. However, high speed op-amps will still be needed to implement the current generators and differential amplifiers. Other approaches are possible if SMD devices are used. Custom designed input circuits were used to make tetrapolar impedance measurements using a 3-terminal single chip impedance measurement device, the AD5933 (Seoane et al., 2008; Margo et al., 2013). A similar approach was used to create a wireless device for lung capacity screening (Pino et al., 2019). Restricting the upper frequency limit to 100 kHz would allow the device to be made from off-the-shelf components that met our component selection criteria, but would exclude measurements where higher frequency transfer impedance changes are reported (Huerta-Nuñez et al., 2019).

The percentage of measurement error of the prototype multi-frequency FIM was below 5% in the frequency range 10–633 kHz for resistive phantoms greater than 10 Ω . For Cole-Cole phantom the error was below 4% except 160 and 296 kHz. But for measurements at 1,033 kHz and impedance below 10 Ω in resistive phantom, the error is around 10% which

is a limitation. The measurement accuracy problem at 1 MHz was the result of the limited range of electronic devices, particularly the non-availability of high speed and low noise op-amps. The problem of stray capacitance cannot be ignored at this frequency and optimizing circuit layout may provide some improvement in performance. The lack of suitable op-amps and passive electronic components with higher tolerance in a low resource setting was a considerable challenge in achieving the final design. As already stated, many multi-frequency impedance measurement systems have used some form of digital demodulation (e.g., Wilson et al., 2001) and the considerable challenge in using analogue demodulation must be emphasised.

The measurement resolution of the designed multi-frequency FIM system is 0.1 Ω . According to Brown et al., respiratory and cardiac related impedance change in the thorax region is around 1.5 and 0.08 Ω , respectively, (Brown et al., 1994). The resolution of the designed multi-frequency FIM system is therefore adequate for monitoring respiratory related changes, but may not be suitable for monitoring cardiac related impedance changes without signal averaging.

The frame rate of the impedance measurement system based on analogue synchronous peak detector was determined from the clock speed of the microcontroller and was found to be greater than 45 fps. This is above the specified frame rate which allows impedance measurements on the thorax region avoiding dynamic changes due to respiration.

CONCLUSION

A multi-frequency FIM system capable of selecting all three version of FIM electrode configuration in the frequency range 10 kHz-1 MHz is described. The multi-frequency FIM system has been developed with the aim of assessing the utility of FIM in diagnosing lung diseases, breast tumour and measuring abdominal fat thickness. Pneumonia, Tuberculosis, edema are

common lung diseases in developing countries, especially amongst children (Izadnegahdar et al., 2013; Jenkins, 2016). So a small, low cost, non-invasive system that can be maintained locally has the potential to benefit a large number of people, particularly those living in the rural areas where modern healthcare facilities and transport are limited. The device meets the EU and UK safety standards for electro-medical equipment. The performance and safety standards of the measurement device described in this paper are adequate to undertake field trials of FIM in the areas of lung disorders, abdominal fat thickness and breast cancer studies.

DATA AVAILABILITY STATEMENT

The original contributions presented in the study are included in the article/Supplementary Material, further inquiries can be directed to the corresponding author.

AUTHOR CONTRIBUTIONS

MK: Methodology, Investigation, Formal Analysis, Writing–Original Draft; AW: Visualization, Validation, Review and Editing, Supervision; KR: Visualization, Validation, Review and Editing, Supervision.

FUNDING

One of the authors MK gratefully acknowledges the support from the Commonwealth Scholarship Commission (CSC) in the United Kingdom (CSC1163262). The authors also acknowledge the International Science Program (ISP) (IPPS BAN04), Uppsala University, Sweden for partial financial support.

REFERENCES

- AAMI (1993). *American National Standard, Safe Current Limits for Electromedical Apparatus* ANSI/AAMI ES1-1993. Arlington, Va: Association for the Advancement of Medical Instrumentation.
- Abdul, S., Brown, B. H., Milnes, P., and Tidy, J. A. (2006). The Use of Electrical Impedance Spectroscopy in the Detection of Cervical Intraepithelial Neoplasia. *Int. J. Gynecol. Cancer* 16 (5), 1823–1832. doi:10.1136/ijgc-00009577-200609000-0001610.1111/j.1525-1438.2006.00651.x
- Adler, A., and Boyle, A. (2017). Electrical Impedance Tomography: Tissue Properties to Image Measures. *IEEE Trans. Biomed. Eng.* 64 (11), 2494–2504. doi:10.1109/TBME.2017.2728323
- Amin, A. A., Parvin, S., Kadir, M. A., Tahmid, T., Alam, S. K., and Siddique-e Rabbani, K. (2014). Classification of Breast Tumour Using Electrical Impedance and Machine Learning Techniques. *Physiol. Meas.* 35 (6), 965–974. doi:10.1088/0967-3334/35/6/965
- Anand, G., Yu, Y., Lowe, A., and Kalra, A. (2021). Bioimpedance Analysis as a Tool for Hemodynamic Monitoring: Overview, Methods and Challenges. *Physiol. Meas.* 42 (3), 03TR01. doi:10.1088/1361-6579/abe80e
- Barber, D. C., Brown, B. H., and Freeston, I. L. (1984). “Imaging Spatial Distributions of Resistivity Using Applied Potential Tomography - APT,” in *Information Processing in Medical Imaging*. Editor F. Deconinck (Dordrecht: Springer), 446–462. doi:10.1007/978-94-009-6045-9_26
- Bertemes Filho, P. (2002). *Tissue Characterisation Using an Impedance Spectroscopy Probe*. Sheffield, U K: Doctoral Dissertation, University of Sheffield.
- Bertemes-Filho, P., Negri, L. H., Felipe, A., and Vincence, V. C. (2012). Mirrored Modified Howland Circuit for Bioimpedance Applications: Analytical Analysis. *J. Phys. Conf. Ser.* 407, 012030. doi:10.1088/1742-6596/407/1/012030
- Bertemes-Filho, P., Negri, L. H., and Vincence, V. C. (2016). Designing a Mirrored Howland Circuit with a Particle Swarm Optimisation Algorithm. *Int. J. Electronics* 103 (6), 1029–1037. doi:10.1080/00207217.2015.1082639
- Bioscan, M., II (2021). Maltron Bioscan 920-2-S. Available at: <https://maltronint.com/bioscan-920-2-s/> (Accessed August 1, 2021).
- Bolton, M. P., Ward, L. C., Khan, A., Campbell, I., Nightingale, P., Dewit, O., et al. (1998). Sources of Error in Bioimpedance Spectroscopy. *Physiol. Meas.* 19 (2), 235–245. doi:10.1088/0967-3334/19/2/011
- Brown, B. (2003). Electrical Impedance Tomography (EIT): a Review. *J. Med. Eng. Technology* 27 (3), 97–108. doi:10.1080/0309190021000059687
- Brown, B. H., Smallwood, R. H., Barber, D. C., Lawford, P., and Hose, D. (2017). *Medical Physics and Biomedical Engineering: Medical Science Series*. Boca Raton, Florida, United States: CRC Press.
- Brown, B. H., Barber, D. C., Morice, A. H., and Leathard, A. D. (1994). Cardiac and Respiratory Related Electrical Impedance Changes in the Human Thorax. *IEEE Trans. Biomed. Eng.* 41 (8), 729–734. doi:10.1109/10.310088

- Brown, B. H., Tidy, J. A., Boston, K., Blackett, A. D., Smallwood, R. H., and Sharp, F. (2000b). Relation between Tissue Structure and Imposed Electrical Current Flow in Cervical Neoplasia. *The Lancet* 355 (9207), 892–895. doi:10.1016/s0140-6736(99)09095-9
- Brown, B. H., Wilson, A. J., and Bertemes-Filho, P. (2000a). Bipolar and Tetrapolar Transfer Impedance Measurements from Volume Conductor. *Electron. Lett.* 36 (25), 2060–2062. doi:10.1049/el:20001439
- Castro, J. A., Olmo, A., Pérez, P., and Yúfera, A. (2016). Microcontroller-Based Sinusoidal Voltage Generation for Electrical Bio-Impedance Spectroscopy Applications. *Jcc* 04 (17), 51–58. doi:10.4236/jcc.2016.417003
- Cheng, Z., Carobbio, A. L. C., Soggiu, L., Migliorini, M., Guastini, L., Mora, F., et al. (2020). SmartProbe: a Bioimpedance Sensing System for Head and Neck Cancer Tissue Detection. *Physiol. Meas.* 41 (5), 054003. doi:10.1088/1361-6579/ab8cb4
- Dechent, D., Emonds, T., Stunder, D., Schmiedchen, K., Kraus, T., and Driessen, S. (2020). Direct Current Electrical Injuries: A Systematic Review of Case Reports and Case Series. *Burns* 46 (2), 267–278. doi:10.1016/j.burns.2018.11.020
- Fein, A., Grossman, R. F., Jones, J. G., Goodman, P. C., and Murray, J. F. (1979). Evaluation of Transthoracic Electrical Impedance in the Diagnosis of Pulmonary Edema. *Circulation* 60 (5), 1156–1160. doi:10.1161/01.CIR.60.5.1156
- Gabriel, S., Lau, R. W., and Gabriel, C. (1996). The Dielectric Properties of Biological Tissues: II. Measurements in the Frequency Range 10 Hz to 20 GHz. *Phys. Med. Biol.* 41 (11), 2251–2269. doi:10.1088/0031-9155/41/11/002
- Geselowitz, D. B. (1971). An Application of Electrocardiographic lead Theory to Impedance Plethysmography. *IEEE Trans. Biomed. Eng.* BME-18 (1), 38–41. doi:10.1109/tbme.1971.4502787
- Grando Sirtoli, V., Coelho Vince, V., and Bertemes-Filho, P. (2019). Mirrored Enhanced Howland Current Source with Feedback Control. *Rev. Scientific Instr.* 90 (2), 024702. doi:10.1063/1.5079872
- Grimnes, S., and Martinsen, O. (2008). *Bioelectricity and Bioimpedance Basics*. Cambridge, Massachusetts: Academic Press.
- Hao, Z., Yue, S., Sun, B., and Wang, H. (2017). Optimal Distance of Multi-Plane Sensor in Three-Dimensional Electrical Impedance Tomography. *Computer Assist. Surg.* 22 (Suppl. 1), 326–338. doi:10.1080/24699322.2017.1389412
- Holder, D. S. (2004). *Electrical Impedance Tomography: Methods, History and Applications*. Boca Raton, Florida, United States: CRC Press.
- Huerta-Núñez, L. F. E., Gutierrez-Iglesias, G., Martinez-Cuaztil, A., Mata-Miranda, M. M., Alvarez-Jiménez, V. D., Sánchez-Monroy, V., et al. (2019). A Biosensor Capable of Identifying Low Quantities of Breast Cancer Cells by Electrical Impedance Spectroscopy. *Sci. Rep.* 9 (1), 6419. doi:10.1038/s41598-019-42776-9
- IEC (2004). The general standard IEC 60601-1 - Medical electrical equipment - Part 1: General requirements. European Committee for Electrotechnical Standardization, Pub. By. The Central Secretariat, rue de Stassart 35, B-1050, Brussels, Belgium, The relevant section on patient auxiliary current is 8.7, 1.
- Islam, N., Rabbani, K. S.-e., and Wilson, A. (2010). The Sensitivity of Focused Electrical Impedance Measurements. *Physiol. Meas.* 31 (8), S97–S109. doi:10.1088/0967-3334/31/8/S08
- Izadnegahdar, R., Cohen, A. L., Klugman, K. P., and Qazi, S. A. (2013). Childhood Pneumonia in Developing Countries. *Lancet Respir. Med.* 1 (7), 574–584. doi:10.1016/S2213-2600(13)70075-4
- Jenkins, H. E. (2016). Global burden of Childhood Tuberculosis. *Pneumonia* 8 (1), 1–7. doi:10.1186/s41479-016-0018-6
- Kadir, M. A., Baig, T. N., and Rabbani, K. S.-e. (2015). Focused Impedance Method to Detect Localized Lung Ventilation Disorders in Combination with Conventional Spirometry. *Biomed. Eng. Appl. Basis Commun.* 27 (03), 1550029. doi:10.4015/S1016237215500295
- Kadir, M. A., and Rabbani, K. S.-e. (2018). Use of a Conical Conducting Layer with an Electrical Impedance Probe to Enhance Sensitivity in Epithelial Tissues. *J. Electr. Bioimpedance* 9 (1), 176–183. doi:10.2478/joeb-2018-0022
- Leeming, M. N., Ray, C., and Howland, W. S. (1970). Low-voltage, Direct-Current burns. *JAMA* 214 (9), 1681–1684. doi:10.1001/jama.214.9.1681
- Lukaski, H. C., Vega Diaz, N., Talluri, A., and Nescolarde, L. (2019). Classification of Hydration in Clinical Conditions: Indirect and Direct Approaches Using Bioimpedance. *Nutrients* 11 (4), 809. doi:10.3390/nu11040809
- Mansouri, S., Alhadidi, T., and Ben Azouz, M. (2020). Breast Cancer Detection Using Low-Frequency Bioimpedance Device. *Bctt* Vol. 12, 109–116. doi:10.2147/bctt.s274421
- Margo, C., Katrib, J., Nadi, M., and Rouane, A. (2013). A Four-Electrode Low Frequency Impedance Spectroscopy Measurement System Using the AD5933 Measurement Chip. *Physiol. Meas.* 34 (4), 391–405. doi:10.1088/0967-3334/34/4/391
- Martinsen, Ø. G., and Grimnes, S. (2009). “The Concept of Transfer Impedance in Bioimpedance Measurements,” in *4th European Conference of the International Federation for Medical and Biological Engineering* (Berlin/Heidelberg, Germany: Springer), 1078–1079. doi:10.1007/978-3-540-89208-3_257
- McEwan, A., Cusick, G., and Holder, D. S. (2007). A Review of Errors in Multi-Frequency EIT Instrumentation. *Physiol. Meas.* 28 (7), S197–S215. doi:10.1088/0967-3334/28/7/s15
- Morais, C. C. A., Safaee Fakhri, B., De Santis Santiago, R. R., Di Fenza, R., Marutani, E., Gianni, S., et al. (2021). Bedside Electrical Impedance Tomography Unveils Respiratory “Chimera” in COVID-19. *Am. J. Respir. Crit. Care Med.* 203 (1), 120–121. doi:10.1164/rccm.202005-1801im
- Mulasi, U., Kuchnia, A. J., Cole, A. J., and Earthman, C. P. (2015). Bioimpedance at the Bedside. *Nutr. Clin. Pract.* 30 (2), 180–193. doi:10.1177/0884533614568155
- Nguyen, D. T., Kosobrodov, R., Barry, M. A., Chik, W., Jin, C., Oh, T. I., et al. (2013). Electrode-Skin Contact Impedance: *In Vivo* Measurements on an Ovine Model. *J. Phys. Conf. Ser.* 434, 012023. doi:10.1088/1742-6596/434/1/012023
- Pallas-Areny, R., and Webster, J. G. (1993). AC Instrumentation Amplifier for Bioimpedance Measurements for Bioimpedance Measurements. *IEEE Trans. Biomed. Eng.* 40 (8), 830–833. doi:10.1109/10.238470
- Petersen, F. J., Ferdous, H., Kalvøy, H., Martinsen, Ø. G., and Høgetveit, J. O. (2014). Comparison of Four Different FIM Configurations-A Simulation Study. *Physiol. Meas.* 35 (6), 1067–1082. doi:10.1088/0967-3334/35/6/1067
- Pino, E. J., Gomez, B., Monsalve, E., and Aqueveque, P. (2019). “Wireless Low-Cost Bioimpedance Measurement Device for Lung Capacity Screening,” in *2019 41st Annual International Conference of the IEEE Engineering in Medicine and Biology Society (EMBC)* (Piscataway, New Jersey, United States: IEEE), 1187–1190. doi:10.1109/EMBC.2019.8857387
- Rabbani, K. S.-e. (2018). “Focused Impedance Method: Basics and Applications,” in *Bioimpedance in Biomedical Applications and Research*. Editors F. Simini and P. Bertemes-Filho (Cham: Springer), 137–185. doi:10.1007/978-3-319-74388-2_9
- Rabbani, K. S., Hassan, M., and Kiber, A. (1996). 3D Object Localization Using EIT Measurements at Two Levels. *Physiol. Meas.* 17 (3), 189–199. doi:10.1088/0967-3334/17/3/005
- Rabbani, K. S., and Kabir, A. M. B. H. (1991). Studies on the Effect of the Third Dimension on a Two-Dimensional Electrical Impedance Tomography System. *Clin. Phys. Physiol. Meas.* 12 (4), 393–402. doi:10.1088/0143-0815/12/4/009
- Rabbani, K. S., and Karal, M. A. S. (2008). A New Four-Electrode Focused Impedance Measurement (FIM) System for Physiological Study. *Ann. Biomed. Eng.* 36 (6), 1072–1077. doi:10.1007/s10439-008-9470-7
- Rabbani, K. S., Sarker, M., Akond, M. H. R., and Akter, T. (1999). Focused Impedance Measurement (FIM): A New Technique with Improved Zone Localization. *Ann. NY Acad Sci* 873 (1), 408–420. doi:10.1111/j.1749-6632.1999.tb09490.x
- Rosell, J., and Riu, P. (1992). Common-mode Feedback in Electrical Impedance Tomography. *Clin. Phys. Physiol. Meas.* 13 (A), 11–14. doi:10.1088/0143-0815/13/a/002
- Roy, S. K., Karal, M. A. S., Kadir, M. A., and Rabbani, K. S.-e. (2019). A New Six-Electrode Electrical Impedance Technique for Probing Deep Organs in the Human Body. *Eur. Biophys. J.* 48 (8), 711–719. doi:10.1007/s00249-019-01396-x
- Sanchez, B., Vandersteen, G., Bragos, R., and Schoukens, J. (2012). Basics of Broadband Impedance Spectroscopy Measurements Using Periodic Excitations. *Meas. Sci. Technol.* 23 (10), 105501. doi:10.1088/0957-0233/23/10/105501
- Scientific Instruments (2019). Sciospec Sciospec ISX-5, Scientific Instruments GmbH. Available at: <https://www.sciospec.com/product/isx-5/> (Accessed August 1, 2021).
- Soeane, F., Ferreira, J., Sanchéz, J. J., and Bragós, R. (2008). An Analog Front-End Enables Electrical Impedance Spectroscopy System On-Chip for Biomedical

- Applications. *Physiol. Meas.* 29 (6), S267–S278. doi:10.1088/0967-3334/29/6/S23
- Surovy, N. J., Billah, M. M., Haowlader, S., Al-Quaderi, G. D., and Rabbani, K. S.-e. (2012). Determination of Abdominal Fat Thickness Using Dual Electrode Separation in the Focused Impedance Method (FIM). *Physiol. Meas.* 33 (5), 707–718. doi:10.1088/0967-3334/33/5/707
- Tidy, J. A., and Brown, B. H. (2021). Clinical Utility of ZedScan when Used as an Adjunct to Colposcopy. *Indian J. Gynecol. Oncolog* 19 (3), 55. doi:10.1007/s40944-021-00540-w
- Vermeiren, E., Ysebaert, M., Van Hoorenbeeck, K., Bruyndonckx, L., Van Dessel, K., Van Helvoirt, M., et al. (2021). Comparison of Bioimpedance Spectroscopy and Dual Energy X-ray Absorptiometry for Assessing Body Composition Changes in Obese Children during Weight Loss. *Eur. J. Clin. Nutr.* 75 (1), 73–84. doi:10.1038/s41430-020-00738-9
- Wilson, A. J., Milnes, P., Waterworth, A. R., Smallwood, R. H., and Brown, B. H. (2001). Mk3.5: a Modular, Multi-Frequency Successor to the Mk3a EIS/EIT System. *Physiol. Meas.* 22 (1), 49–54. doi:10.1088/0967-3334/22/1/307
- Worapishet, A., Demosthenous, A., and Liu, X. (2011). A CMOS Instrumentation Amplifier with 90-dB CMRR at 2-MHz Using Capacitive Neutralization: Analysis, Design Considerations, and Implementation. *IEEE Trans. Circuits Syst.* 58 (4), 699–710. doi:10.1109/TCSI.2010.2078850
- Yang, L., Dai, M., Xu, C., Zhang, G., Li, W., Fu, F., et al. (2017). The Frequency Spectral Properties of Electrode-Skin Contact Impedance on Human Head and its Frequency-dependent Effects on Frequency-Difference EIT in Stroke Detection from 10Hz to 1MHz. *PLoS one* 12 (1), e0170563. doi:10.1371/journal.pone.0170563
- Ye, G., Lim, K. H., George, R. T., Jr, Ybarra, G. A., Joines, W. T., and Liu, Q. H. (2008). 3D EIT for Breast Cancer Imaging: System, Measurements, and Reconstruction. *Microw. Opt. Technol. Lett.* 50 (12), 3261–3271. doi:10.1002/mop.23932
- Zhang, K., Li, M., Yang, F., Xu, S., and Abubakar, A. (2019). Three-dimensional Electrical Impedance Tomography with Multiplicative Regularization. *IEEE Trans. Biomed. Eng.* 66 (9), 2470–2480. doi:10.1109/TBME.2018.2890410

Conflict of Interest: The authors declare that the research was conducted in the absence of any commercial or financial relationships that could be construed as a potential conflict of interest.

Publisher's Note: All claims expressed in this article are solely those of the authors and do not necessarily represent those of their affiliated organizations, or those of the publisher, the editors and the reviewers. Any product that may be evaluated in this article, or claim that may be made by its manufacturer, is not guaranteed or endorsed by the publisher.

Copyright © 2021 Kadir, Wilson and Rabbani. This is an open-access article distributed under the terms of the Creative Commons Attribution License (CC BY). The use, distribution or reproduction in other forums is permitted, provided the original author(s) and the copyright owner(s) are credited and that the original publication in this journal is cited, in accordance with accepted academic practice. No use, distribution or reproduction is permitted which does not comply with these terms.